NACA

RESEARCH MEMORANDUM

PRESSURE DISTRIBUTION AT LOW SPEED ON A MODEL INCORPORATING A W WING WITH ASPECT RATIO 6, 45° SWEEP, TAPER RATIO 0.6, AND AN NACA 65A009 AIRFOIL SECTION

By Edward C. Polhamus and Albert G. Few, Jr.

Langley Aeronautical Laboratory
Langley Field, Va.

NATIONAL ADVISORY COMMITTEE
FOR AERONAUTICS

WASHINGTON

August 7, 1952

NATIONAL ADVISORY COMMITTEE FOR AERONAUTICS

RESEARCH MEMORANDUM

PRESSURE DISTRIBUTION AT LOW SPEED ON A MODEL INCORPORATING A W WING WITH ASPECT RATIO 6, 45° SWEEP, TAPER RATIO 0.6, AND AN NACA 65A009 AIRFOIL SECTION

By Edward C. Polhamus and Albert G. Few, Jr.

SUMMARY

This paper contains results of pressure-distribution measurements at low speed on a wing-fuselage combination having a wing of W plan form with aspect ratio 6, 45° sweep, taper ratio 0.6, and an NACA 65A009 airfoil section placed parallel to the plane of symmetry. The test Reynolds numbers ranged from 1,190,000 to 1,580,000.

The chordwise pressure distributions, which were determined at various spanwise stations, indicate that a vortex type of flow exists over the wing at moderate and high angles of attack. The strength and location of this vortex were appreciably affected by changing the angle of sideslip. The experimental chordwise and spanwise load distributions at an angle of attack of 2.3° were in fair agreement with theory except near the wing juncture, where there appears to be a mixing and shedding of the boundary layer from the inboard and outboard wing panels. Wake surveys at the juncture indicate a rather large increase in total pressure loss at moderate to high angles of attack.

INTRODUCTION

Composite-plan-form wings made up of sweptback and sweptforward panels have been proposed to alleviate the low-speed stability problems associated with sweptback wings. An investigation made at low speed (ref. 1) indicated that such alleviation was obtained by the use of M and W wings. In a later investigation (ref. 2) it was found that the large unstable shift of the aerodynamic center associated with a 9-percent-thick swept wing in the transonic range was eliminated by the use of an M or W plan form and that, although the drag at zero lift was higher in

the transonic range than for a straight sweptback wing, a fairly large portion of the sweep effect was realized. Recently, it has been pointed out that M and W wings may have an additional advantage over conventional sweptback wings in that the wings of composite plan form should have smaller spanwise twist under air load.

The present paper presents the results of low-speed pressure-distribution measurements of a wing-fuselage configuration incorporating a wing of W plan form. The wing-fuselage combination used for this investigation was the same as that used in an investigation of the low-speed aerodynamic characteristics of a complete airplane configuration employing a W wing reported in reference 3. The present investigation also included wake surveys at several angles of attack for various spanwise positions. Stall patterns obtained from tuft studies on the wing for several angles of attack are also presented.

SYMBOLS

The system of axes employed together with an indication of the positive forces, moments, and angles is presented in figure 1. All pitching-moment coefficients are referred to the quarter-chord of the mean aerodynamic chord. The symbols used in this paper are defined as follows:

C_L	lift coefficient, Lift/qS
C_X	longitudinal-force coefficient, X/qS
C_m	pitching-moment coefficient, $M/qS\bar{c}$
X	longitudinal force along X-axis, lb
M	pitching moment about Y-axis, ft-lb
q	free-stream dynamic pressure, $\rho V^2/2$, lb/sq ft
S	wing area, sq ft
$\bar{c}$	wing mean aerodynamic chord, $\frac{2}{S}\int_0^{b/2} c^2 dy$, ft
P	pressure coefficient, $\frac{p_l - p}{q}$

[redacted]

p_l	local static pressure, lb/sq ft
p	free-stream static pressure, lb/sq ft
ρ	mass density of air, slugs/cu ft
V	free-stream velocity, ft/sec
c	local wing chord, parallel to plane of symmetry, ft
c_{av}	average wing chord, parallel to plane of symmetry, ft
β	angle of sideslip, positive when relative wind is from the right, deg
α	angle of attack, measured parallel to plane of symmetry, deg
d	distance rearward of fuselage nose measured parallel to plane of symmetry, ft
x	distance behind local wing leading edge measured parallel to plane of symmetry, ft
L	actual length of fuselage, ft
b	wing span, ft
y	spanwise distance measured perpendicular to plane of symmetry, ft
c_n	section normal-force coefficient
z	height above wing chord plane, ft
ΔH	loss in total pressure, lb/sq ft
ΔP	pressure-difference coefficient, $P_{upper} - P_{lower}$

APPARATUS AND METHODS

A three-view drawing of the model as tested is presented as figure 2. The wing had a W plan form of aspect ratio 6 with 45° sweep, a taper ratio of 0.6, and an NACA 65A009 airfoil section placed parallel to the plane of symmetry. The ordinates of the airfoil section are

[redacted]

presented in figure 3. The fuselage had a fineness ratio of 10, achieved by cutting off the rear one-sixth of a fineness-ratio-12 body of revolution, the ordinates of which are presented in figure 3. The fuselage was constructed of wood and the wing was constructed of wood cycle-welded to a steel spar.

Pressure orifices were installed in the wing at 13 chordwise positions for each of six spanwise stations shown in figure 4. In order to reduce the number of orifices and manometer boards needed, orifices were installed in only the upper surface of the wing and the model, which was symmetrical, was tested at both positive and negative angles of attack in order to obtain data representative of both the upper and lower surfaces for the wing at positive angles of attack. Pressure measurements at the three inboard spanwise stations were made on the right wing while those for the three outboard stations were measured on the left wing for simplicity of installation. Pressure orifices were also installed in the fuselage at 21 stations along each of three meridian lines as illustrated in figure 4. Figure 5 shows the model mounted on the center support strut.

For use in wing wake surveys a rake consisting of a series of total-pressure tubes extending over the entire wake at moderate angles of attack was mounted at a distance equal to $0.806b/2$ rearward of the quarter-chord of the mean aerodynamic chord.

TESTS

The pressure-distribution tests were made in the Langley 300 MPH 7- by 10-foot tunnel at a dynamic pressure of 39.96 pounds per square foot which for average test conditions corresponds to a Mach number of 0.17 and to a Reynolds number of 1,190,000 based on the mean aerodynamic wing chord. Force tests and wake surveys were made at a dynamic pressure of 73.12 and 71.11 pounds per square foot, respectively, which for average test conditions corresponds to a Mach number of about 0.22 and a Reynolds number of about 1,580,000. Several tests were made at a Reynolds number of about 1,580,000 and an angle of attack of 2.3° in order to compare experimental and theoretical chordwise and spanwise load distributions.

With the model at a given angle of attack, a record was taken of the pressures at the orifices by photographing the multiple-tube manometer to which the orifices were connected.

CORRECTIONS

The angle of attack, drag, and pitching-moment data have been corrected for jet-boundary induced upwash on the basis of unswept wings (ref. 4) and for the tares caused by the model support strut. Calculations have shown that the effects of sweep on these jet-boundary corrections are negligible. No attempt has been made to correct the pressure data for the slight spanwise and chordwise variation of the jet-boundary induced upwash. All coefficients have been corrected for blocking by the model and its wake by the method of reference 5. Tunnel-air-flow misalinement has been accounted for in the computation of the test data.

RESULTS AND DISCUSSION

Presentation of Results

The results of this investigation are presented in the figures tabulated below:

Aerodynamic Characteristics

The low-speed aerodynamic characteristics obtained for the wing-fuselage combination at zero angle of sideslip are presented in figure 6. All pitching-moment coefficients are referred to the quarter-chord of the mean aerodynamic chord. While the data of figure 6 are

[redacted]

included mainly for the purpose of correlation of the pressure data with the force data, there are a few interesting points illustrated which should be mentioned. It will be noted that the pitching-moment data illustrate the advantage of W wings with regard to stability inasmuch as the pitching-moment curve is essentially linear throughout the lift range; whereas a sweptback wing having the same sweep and aspect ratio would be expected to have a large unstable break at a lift coefficient of about 0.50 and continuing to the stall (see ref. 6). It is also interesting to note that for this particular wing-fuselage combination the lift-curve slope is in good agreement with the theoretical wing-alone results calculated by the method of reference 7. The theoretical lift-curve slope is 0.062 while the experimental wing-fuselage lift-curve slope is 0.063. The theoretical wing-alone aerodynamic-center location is at 31.4 percent of the mean aerodynamic chord, while the experimental wing-fuselage aerodynamic-center location is at 31.0 percent of the mean aerodynamic chord.

Pressure Distribution on the Wing

Wing pressure distribution and wake surveys, $\beta = 0^\circ$.- The chordwise pressure distributions at six semispan stations for various angles of attack are presented in figures 7 to 12. Wake surveys at several angles of attack are presented in figure 13 for various spanwise positions at a distance equal to 0.806b/2 rearward of the quarter-chord of the mean aerodynamic chord. The wake surveys are presented as plots of total-pressure loss $\Delta H/q$ against height above wing chord plane z/c. The chordwise pressure distributions at low angles of attack (figs. 7 and 8), in general, are normal. At an angle of attack of 8.6° (fig. 9), there is an indication of a vortex-type flow over the inboard panel of the wing. This is reflected in the pressure distribution at the leading edge of the 20- to 50-percent-semispan stations. This type of flow phenomena has been reported in reference 8. Wake surveys in this region (fig. 13) at a comparable angle of attack show large increases in total-pressure loss, which is indicative of separation. At 8.6° angle of attack there appears to be no vortex flow on the outboard panel. At 12.7° angle of attack (fig. 10), the vortex pattern on the inboard panel has moved inboard and a second vortex appears to have formed on the outboard panel. At the higher angles of attack the inboard panel has stalled and the outboard stall pattern progresses toward the tip. The delay in the formation of the vortex on the outboard panel is probably due to the fact that the effective angle of attack is considerably less on the outboard panel than on the inboard panel.

Experimental and theoretical spanwise load distribution.- A comparison of the experimental and theoretical spanwise load distributions is presented in figure 14. The experimental results are for an angle of attack of 2.3° and the theoretical results were calculated by the method

of reference 7. In general, the agreement is rather poor with the experimental loading having a rather large dip at the midsemispan station. However, the experimental loading does substantiate the rather rapid load gradient from the midsemispan station out to the wing tip.

Experimental and theoretical chordwise load distribution.- Comparisons between the experimental and thin-airfoil-theory chordwise load distributions $\left(\Delta P = 4\alpha_l\sqrt{\frac{1 - \frac{x}{c}}{x/c}}\right.$, where α_l is the local effective angle of attack expressed in radians, which was determined from the theoretical spanwise load distribution$\left.\right)$ at an angle of attack of 2.3° are presented in figure 15. The agreement at the two inboard and two outboard stations is fairly good. However, at the 50-percent-semispan and 60-percent-semispan stations the agreement is rather poor especially at the 50-percent-semispan station where there appears to be a rather large camber effect. This may be due to boundary-layer drainage from the inboard and outboard panels with the boundary layer being thicker on the upper surface of the wing.

Effects of sideslip.- The effects on the wing pressure distribution of sideslipping the model are indicated in figures 16 and 17. In the presentation of the data the sign of the sideslip angle has been reversed for the three outboard stations so that figures 16 and 17 may be interpreted as though all pressures were measured on the right wing. Measurements at negative sideslip angles yield results for the trailing wing, and conversely, measurements at positive sideslip angles provide pressure distributions on the leading wing. At angles of attack near zero degrees (fig. 16), the effect of sideslip was to increase the magnitude of the pressure coefficients on the sweptforward panel of the trailing wing and the sweptback panel of the leading wing and to decrease those on the other two panels. This effect is attributed to the change with sideslip angle of the velocity components normal to the leading edge. At an angle of attack of 6.5° (fig. 17), sideslipping the model had a pronounced effect on the strength and location of the vortex near the leading edge. At zero sideslip, a vortex type of flow on the inboard panel was evidenced by broadened leading-edge pressure peaks and rapid pressure recovery just behind the peak. This vortex flow became slightly stronger at negative sideslip angles and weaker at positive sideslip angles. No evidence of this vortex flow exists on the outboard panel at zero or high negative angles of sideslip; however, as the sideslip angle increases positively, a vortex appears somewhat downstream from the leading edge on the inboard end of the outboard panel.

[redacted]

Pressure Distribution on the Fuselage

Pressure distributions on the fuselage in the presence of the wing along each of three meridian lines, as illustrated in figure 4, are given in figure 18, while the pressure distributions along these meridian lines for fuselage alone are presented in figure 19. Figure 18 shows an increase in pressure along the three meridian lines near the region of the wing-fuselage juncture. This pressure rise is somewhat greater on the 15° meridian line and diminishes progressively as the 90° meridian line is approached, indicating a pressure carry-over from the wing. It can be seen from figures 18 and 19 that no significant change occurs in the magnitude of the fuselage pressures except in the immediate vicinity of the wing.

Aerodynamic Section Characteristics

The aerodynamic section normal-force characteristics at zero sideslip for various spanwise stations are presented in figure 20. The angle of attack for maximum values of section normal-force coefficients on the inboard panel decreases considerably toward the juncture, indicative of separation beginning first at the wing juncture and progressing inboard as the angle of attack is increased. Little evidence of separation exists on the outboard panel except near the juncture at the 60-percent-semispan station where the normal-force coefficient breaks at about 10° angle of attack. At the lower angles of attack the normal-force curves for the various semispan stations are fairly linear. The large increase in total-pressure loss in the wake at about an angle of attack of 10° from the 35-percent-semispan station to the 60-percent-semispan station (fig. 13) would seem to substantiate the fact that shedding and mixing of the boundary layer in this region results in flow separation as indicated by the breaks in the normal-force curves at these semispan stations.

Stall Patterns

Stall patterns on the wing, as determined from tuft studies, at various angles of attack are presented as figure 21. Separation at the wing juncture appears to begin at a low angle of attack and progresses inboard more rapidly than it does outboard from the region of the juncture. As has previously been pointed out, this could be attributed to the fact that the effective angle of attack at the outboard panel is less than that of the inboard panel. It can be seen that at moderate to high angles of attack the arrows indicate flow from both the inboard and outboard wing panels in a direction toward the wing juncture where the boundary layer from both panels is mixed and shed off the wing resulting in the large increases in total-pressure loss as shown in figure 13.

[redacted]

CONCLUSIONS

Based on the results of pressure-distribution measurements at low speed on a wing-fuselage configuration having a wing of W plan form with aspect ratio 6, 45° sweep, taper ratio 0.6, and an NACA 65A009 airfoil section parallel to the plane of symmetry, the following conclusions are drawn:

1. A vortex type of flow exists over the wing at moderate and high angles of attack as indicated by the pressure distribution. This vortex first appears on the inboard panels and later forms on the outboard panels as the angle of attack is increased.

2. At a given angle of attack, the strength and location of the vortex are appreciably affected by changing the angle of sideslip.

3. Experimental and theoretical chordwise and spanwise load distributions are in fair agreement except near the wing juncture, where there appears to be a mixing and shedding of the boundary layer from the inboard and outboard wing panels.

4. Wake surveys in the region of the juncture indicate a rather large increase in total-pressure loss at moderate to high angles of attack, while the variations of the wake along the span at the lower angles of attack are rather small except for slight increases in the juncture region.

Langley Aeronautical Laboratory
National Advisory Committee for Aeronautics
Langley Field, Va.

[redacted]

REFERENCES

1. Purser, Paul E., and Spearman, M. Leroy: Wind-Tunnel Tests at Low Speed of Swept and Yawed Wings Having Various Plan Forms. NACA TN 2445, 1951. (Supersedes NACA RM L7D23, 1947.)

2. Campbell, George S., and Morrison, William D., Jr.: A Small-Scale Investigation of "M" and "W" Wings at Transonic Speeds. NACA RM L50H25a, 1950.

3. Polhamus, Edward C., and Becht, Robert E.: Low-Speed Stability Characteristics of a Complete Model With a Wing of W Plan Form. NACA RM L52A25, 1952.

4. Gillis, Clarence L., Polhamus, Edward C., and Gray, Joseph L, Jr.: Charts for Determining Jet-Boundary Corrections for Complete Models in 7- by 10-Foot Closed Rectangular Wind Tunnels. NACA ARR L5G31, 1945.

5. Herriot, John G.: Blockage Corrections for Three-Dimensional-Flow Closed-Throat Wind Tunnels With Consideration of the Effect of Compressibility. NACA Rep. 995, 1950. (Supersedes NACA RM A7B28.)

6. Shortal, Joseph A., and Maggin, Bernard: Effect of Sweepback and Aspect Ratio on Longitudinal Stability Characteristics of Wings at Low Speeds. NACA TN 1093, 1946.

7. Campbell, George S.: A Finite-Step Method for the Calculation of Span Loadings of Unusual Plan Forms. NACA RM L50L13, 1951.

8. Lange, Roy H., Whittle, Edward F., Jr., and Fink, Marvin P.: Investigation at Large Scale of the Pressure Distribution and Flow Phenomena Over a Wing With the Leading Edge Swept Back 47.5° Having Circular-Arc Airfoil Sections and Equipped With Drooped-Nose and Plain Flaps. NACA RM L9G15, 1949.

[redacted]

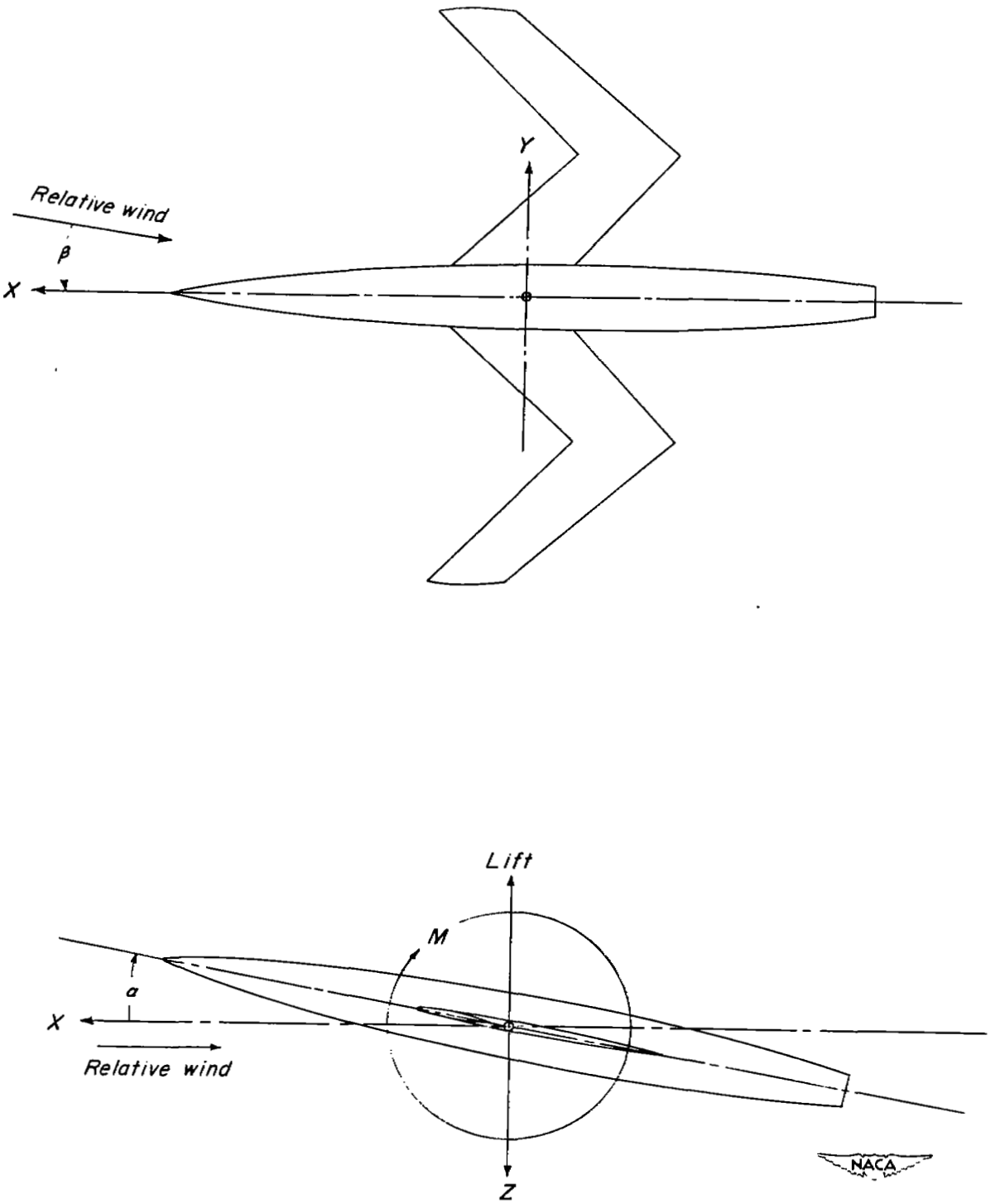

Figure 1.- System of axes. Positive values of forces, moments, and angles are indicated by arrows.

[redacted]

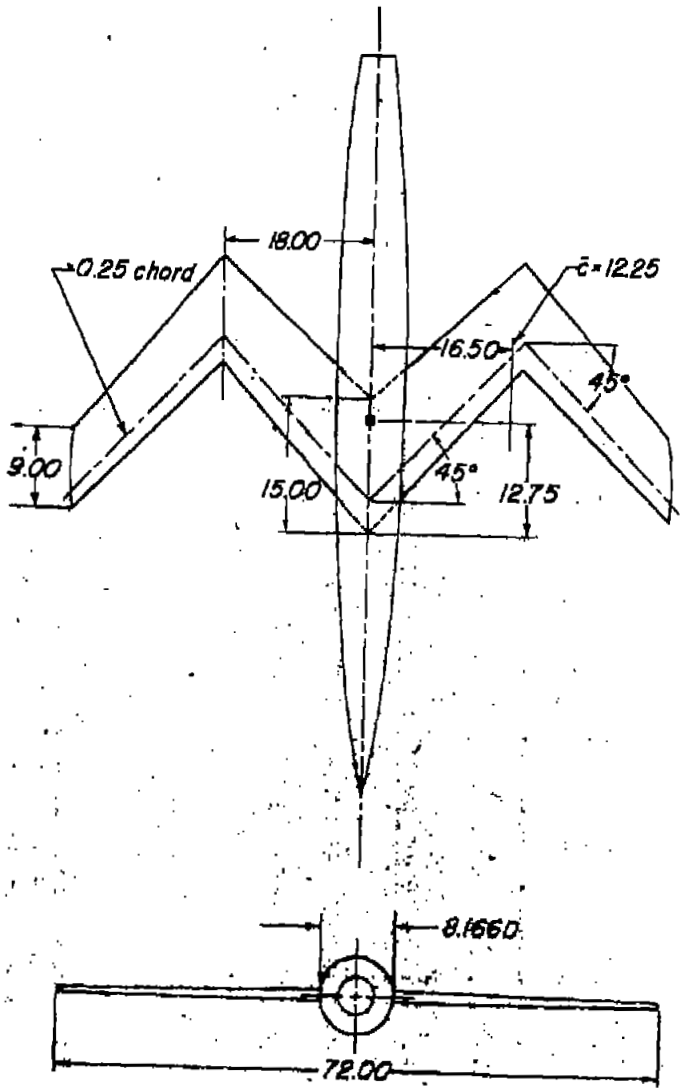

Physical characteristics	
Sweep of inboard panel, deg	45
Sweep of outboard panel, deg	-45
Aspect ratio	6
Taper ratio	0.60
Airfoil section parallel to free stream	NACA 65A009
Area, sq ft	6
Incidence, deg	0
Dihedral, deg	0

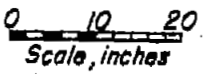

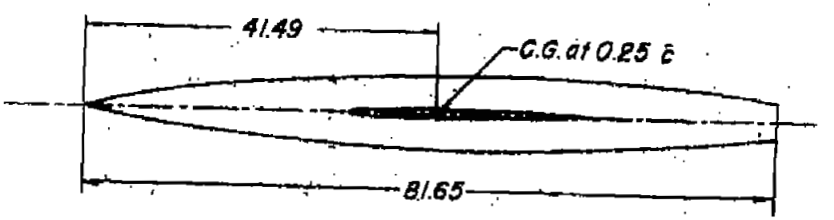

Figure 2.- General arrangement of test model.

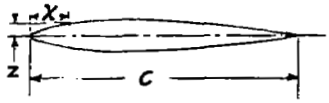

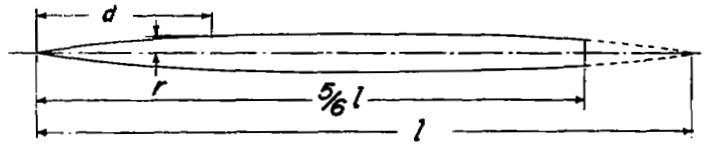

Airfoil ordinates

x (percent c)	z (percent c)
0	0
.5	.688
.75	.835
1.25	1.065
2.5	1.461
5.0	1.968
7.5	2.385
10	2.736
15	3.292
20	3.714
25	4.035
30	4.268
35	4.421
40	4.496
45	4.485
50	4.377
55	4.169
60	3.874
65	3.509
70	3.089
75	2.621
80	2.117
85	1.594
90	1.069
95	.544
100	0.019

L.E. radius .575 percent c
T.E radius .021 percent c

Fuselage ordinates

d/l	r/l
0	0
.005	.002
.008	.003
.013	.004
.025	.007
.050	.012
.075	.016
.100	.020
.150	.026
.200	.031
.250	.035
.300	.037
.350	.039
.400	.041
.450	.041
.500	.042
.550	.041
.600	.040
.650	.038
.700	.036
.750	.031
.800	.025
.833	.021
.850	.019
.900	.011
.950	.004
1.000	0

L.E. radius .0005 l

NACA

Figure 3.- Ordinates for NACA 65A009 airfoil and fuselage of basic fineness ratio 12. Actual fuselage fineness ratio 10 achieved by cutting off the rear 1/6 of the body.

[redacted]

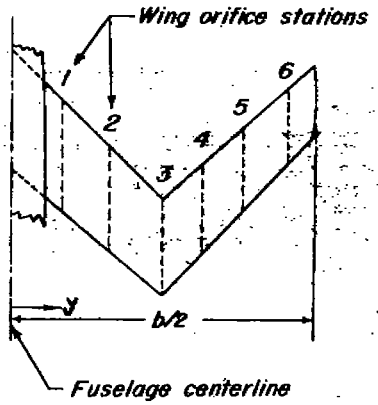

Station	$\frac{y}{b/2}$
1	.10
2	.35
3	.50
4	.80
5	.95
6	.99

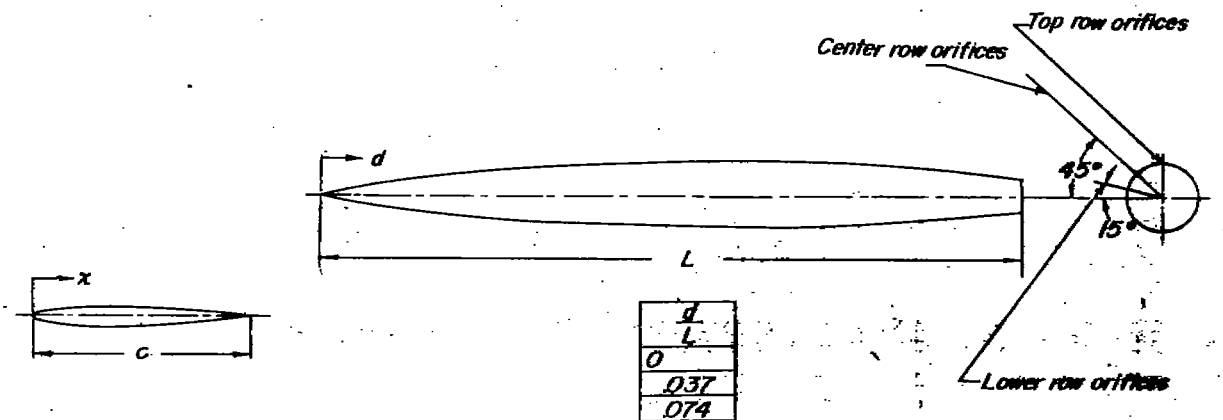

$\frac{x}{c}$
0
.025
.050
.100
.200
.300
.400
.500
.600
.700
.800
.900
1.000

$\frac{d}{L}$
0
.037
.074
.147
.220
.294
.368
.396
.425
.453
.483
.513
.542
.570
.600
.625
.698
.773
.846
.918
.991

Figure 4.- General arrangement and ordinates of pressure orifices on test model.

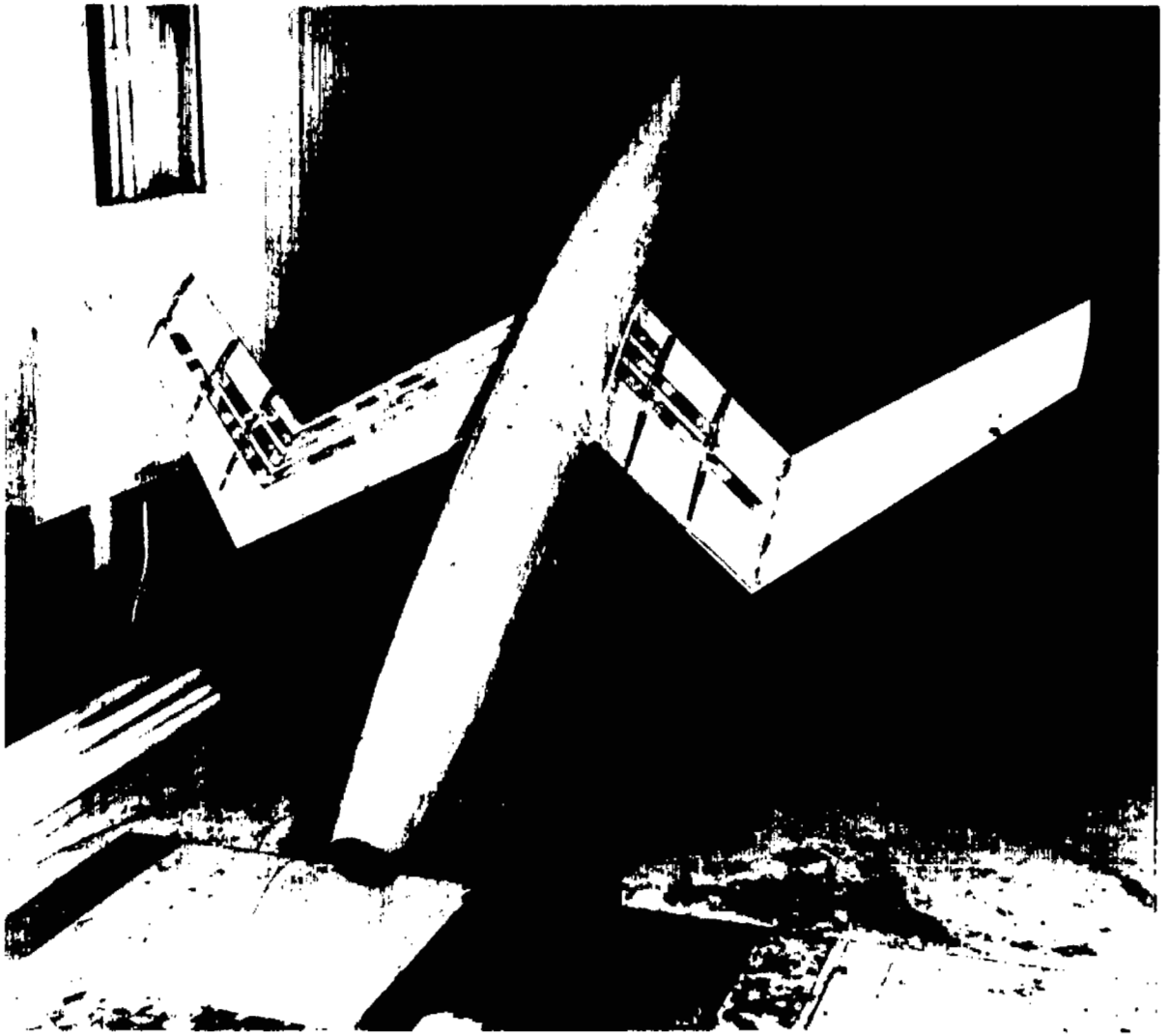

Figure 5.- View of test model as mounted in tunnel.

NACA
L-67337

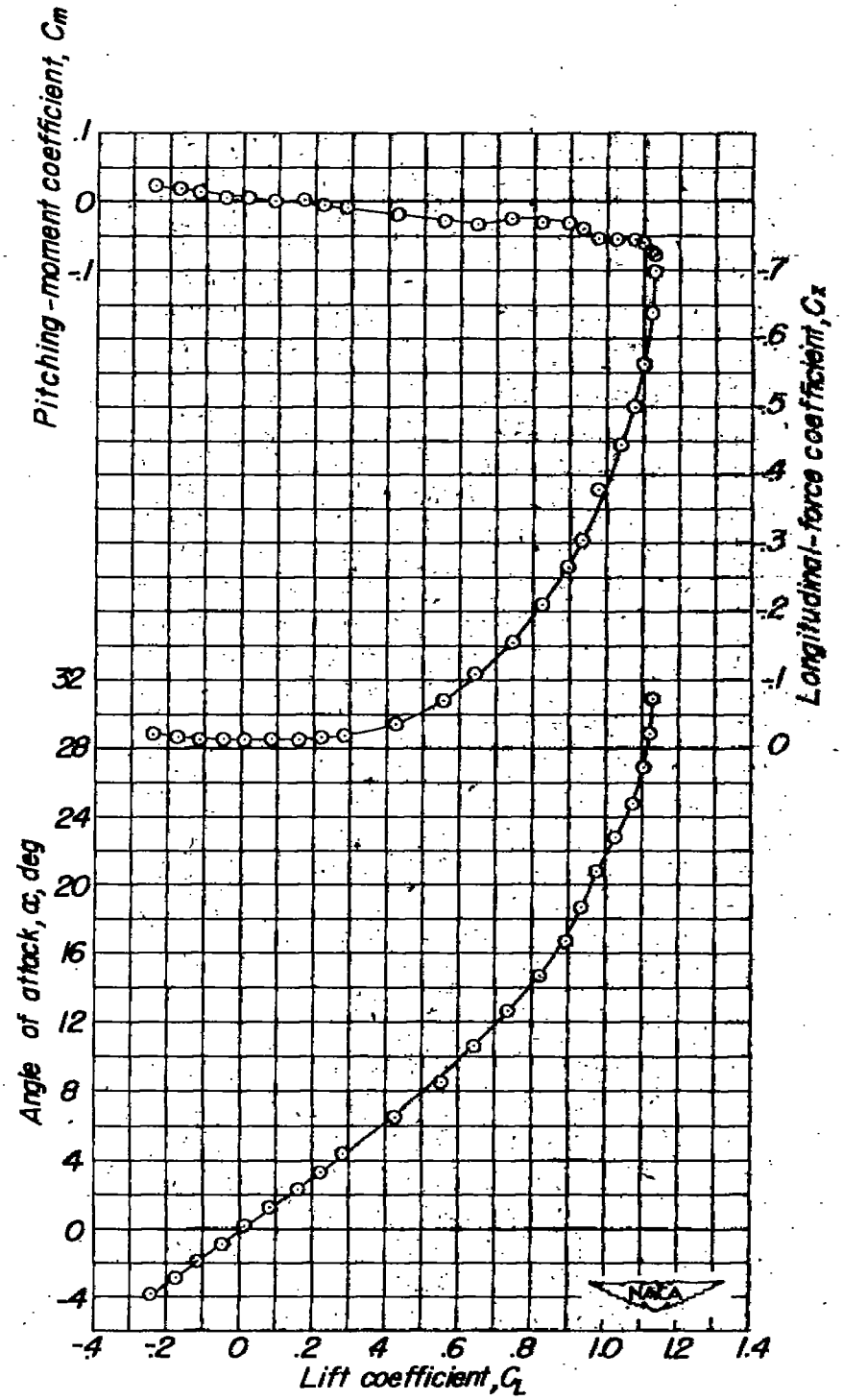

Figure 6.- Aerodynamic characteristics of wing-fuselage combination of test model. $\beta = 0^\circ$.

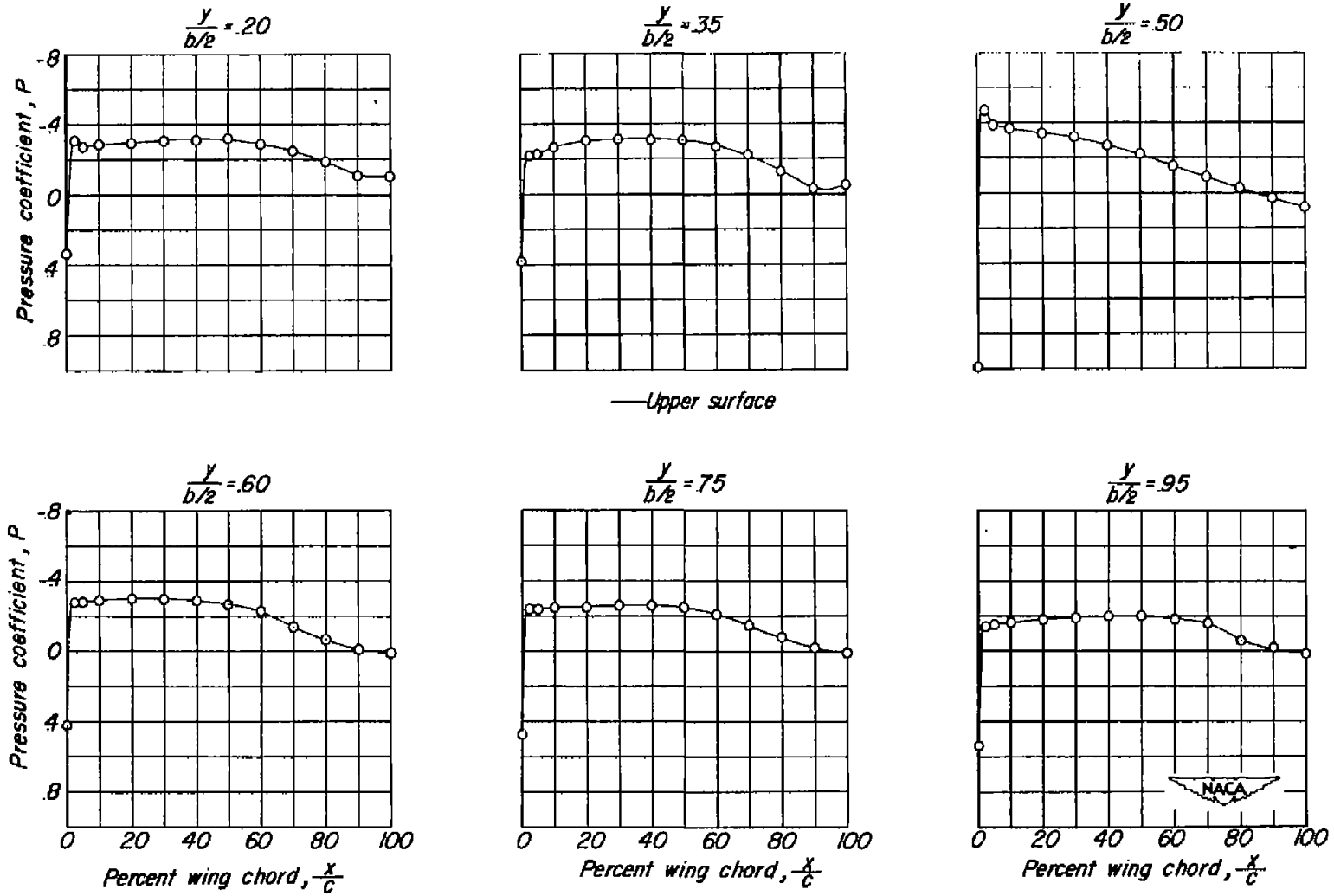

Figure 7.- Pressure distribution on the wing. $\alpha = 0.2^{\circ}$; $\beta = 0^{\circ}$.

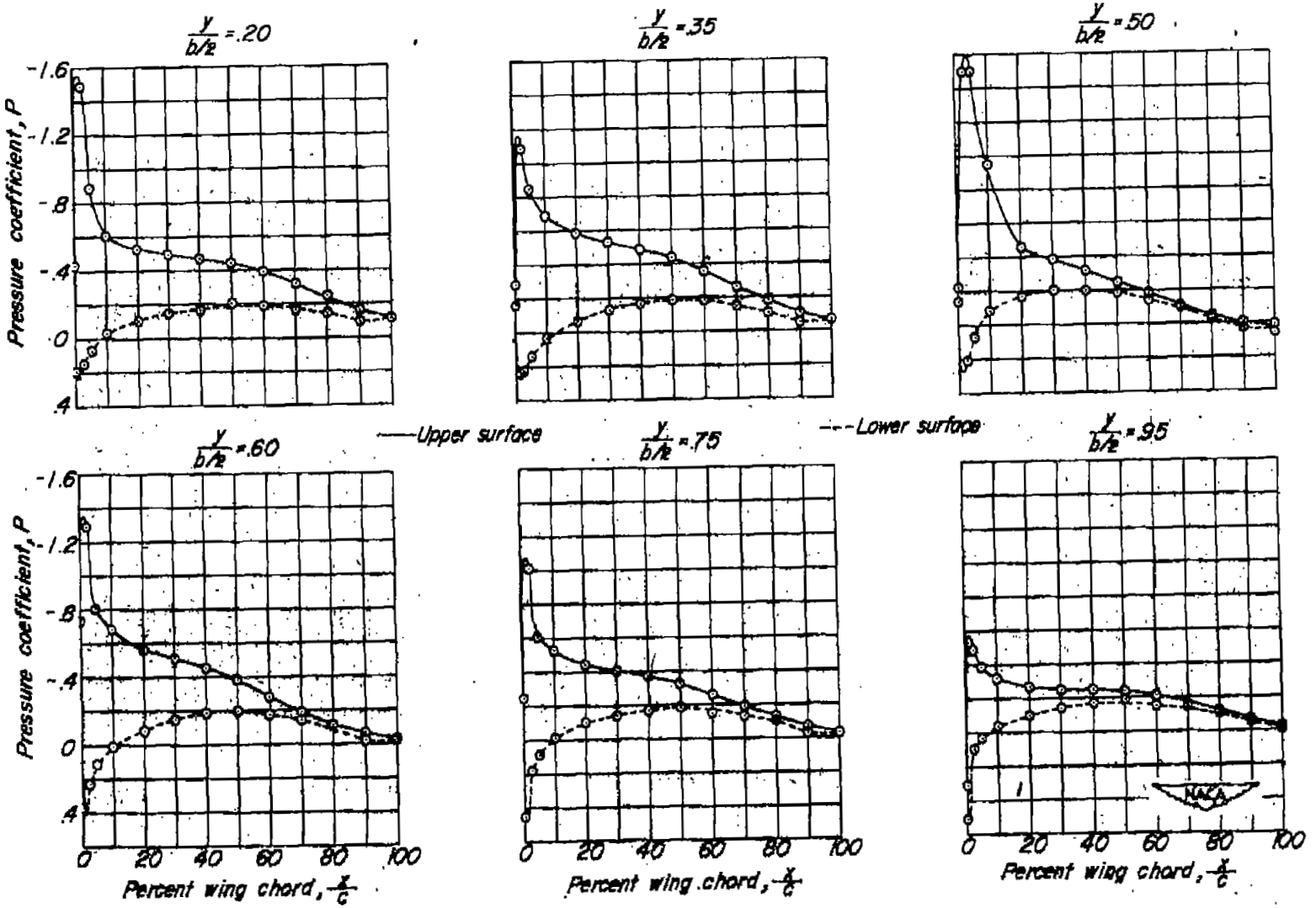

Figure 8.- Pressure distribution on the wing. $\alpha = 4.4^{\circ}$; $\beta = 0^{\circ}$.

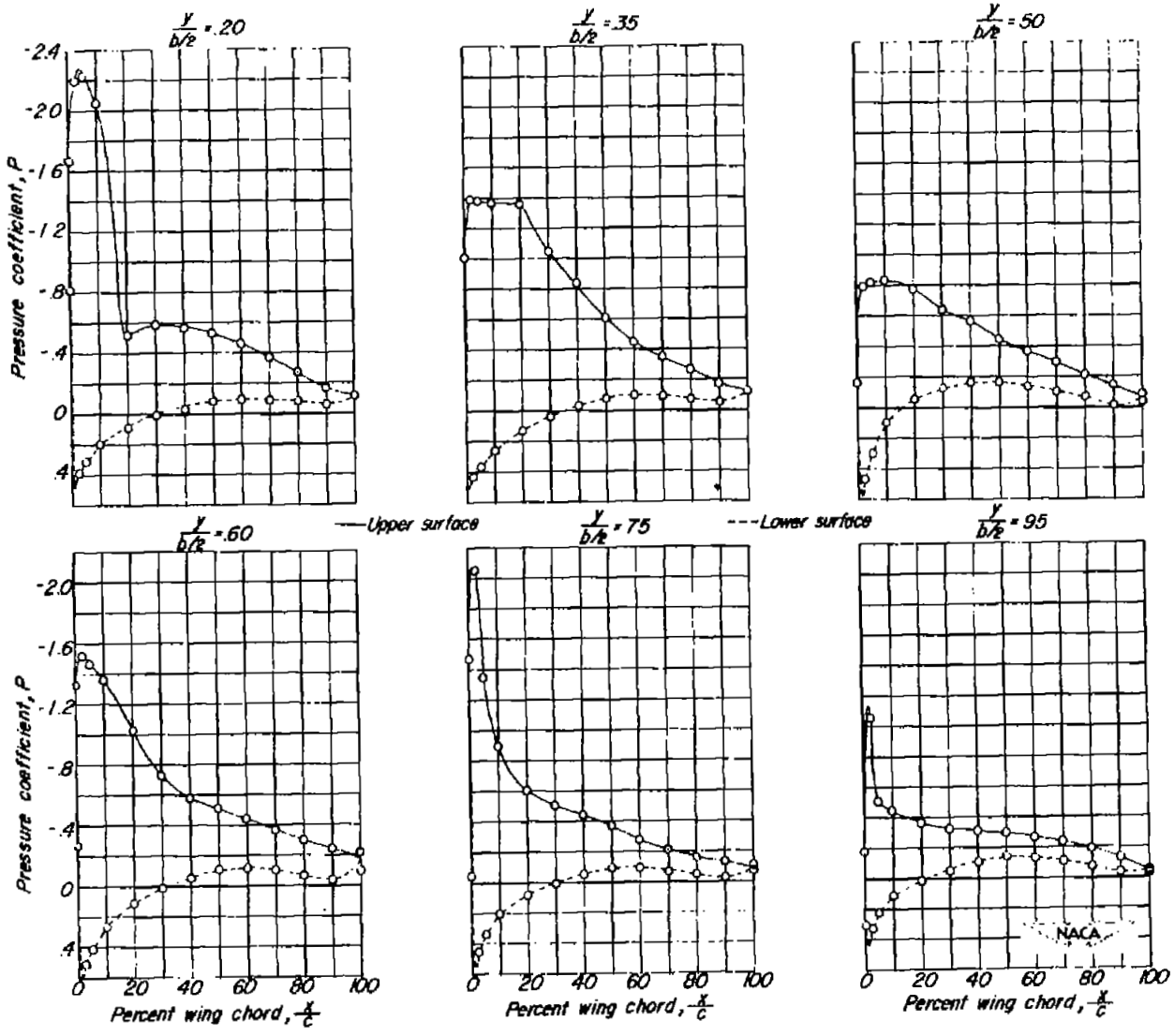

Figure 9.- Pressure distribution on the wing. $\alpha = 8.6^{\circ}$; $\beta = 0^{\circ}$.

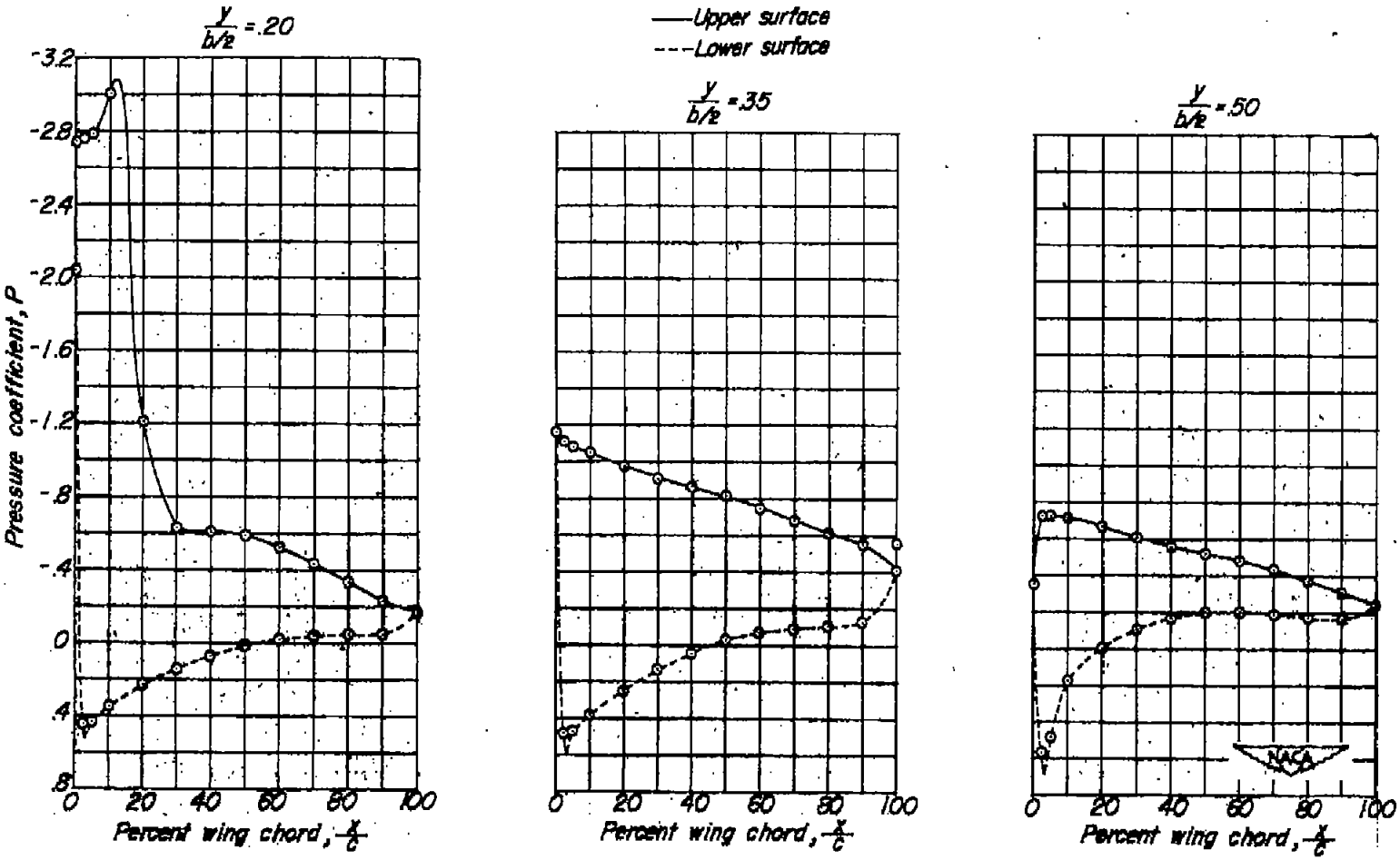

Figure 10.- Pressure distribution on the wing. $\alpha = 12.7^{\circ}$; $\beta = 0^{\circ}$.

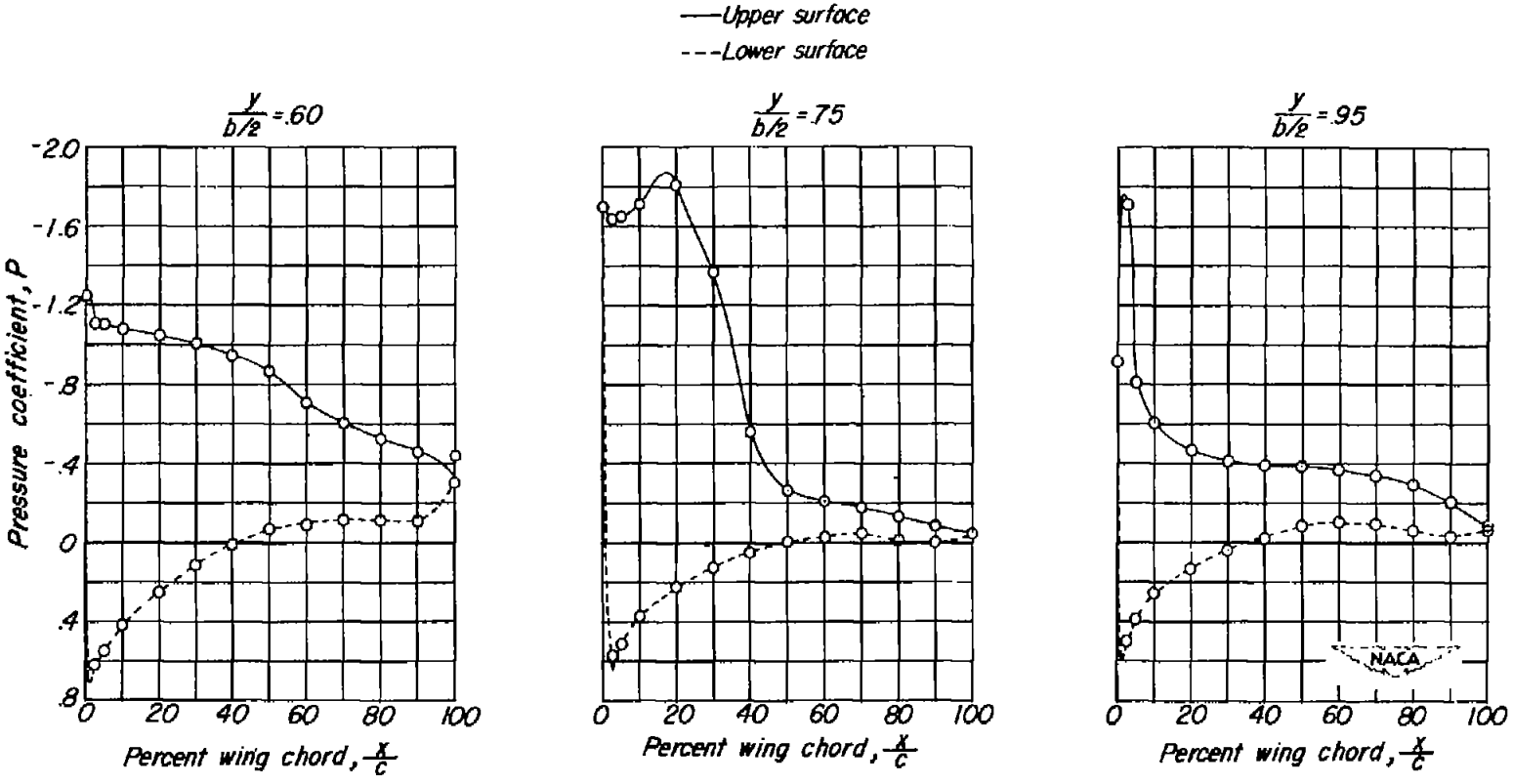

Figure 10.- Concluded.

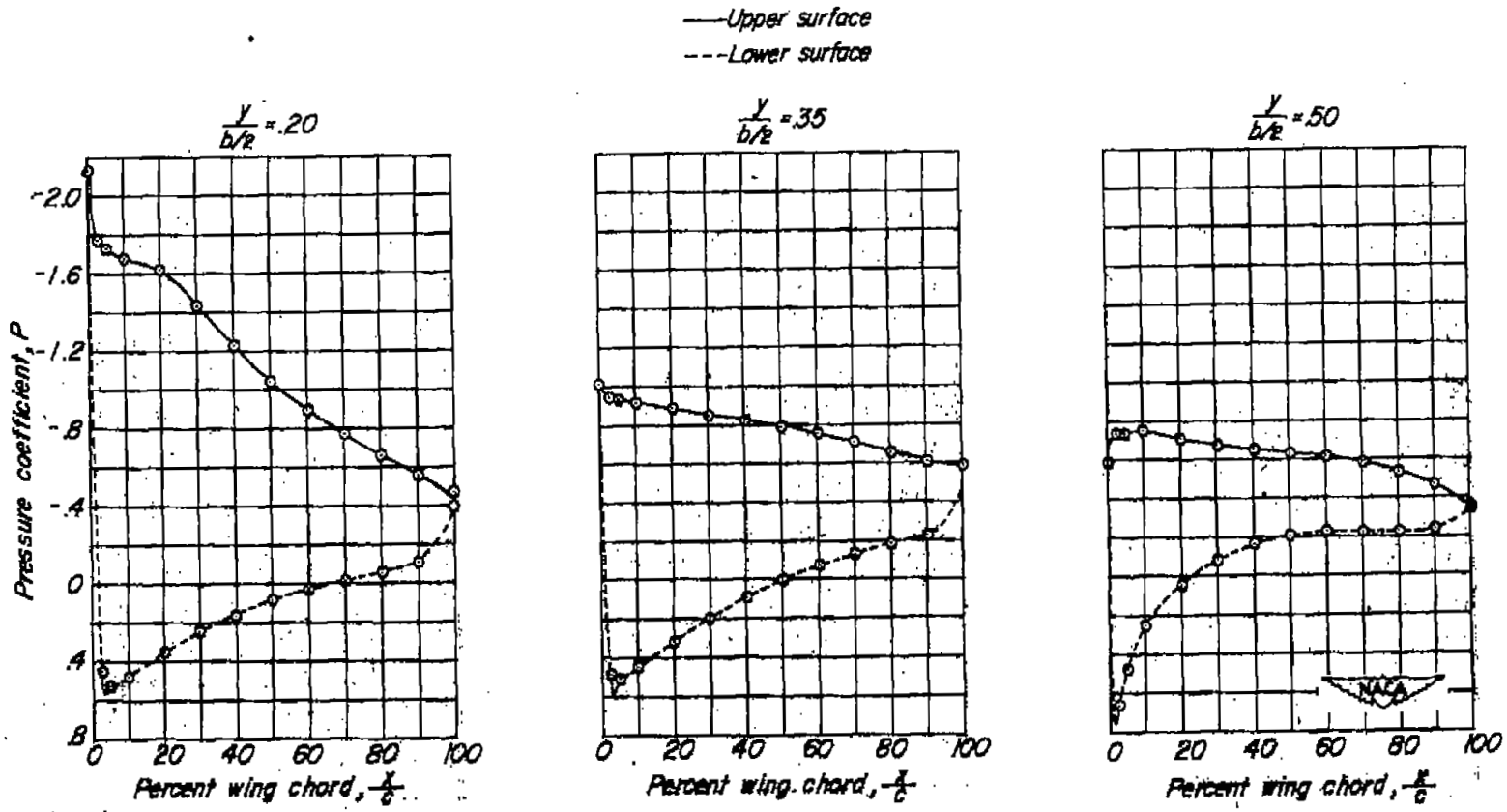

Figure 11.- Pressure distribution on the wing. $\alpha = 16.7^\circ$; $\beta = 0^\circ$.

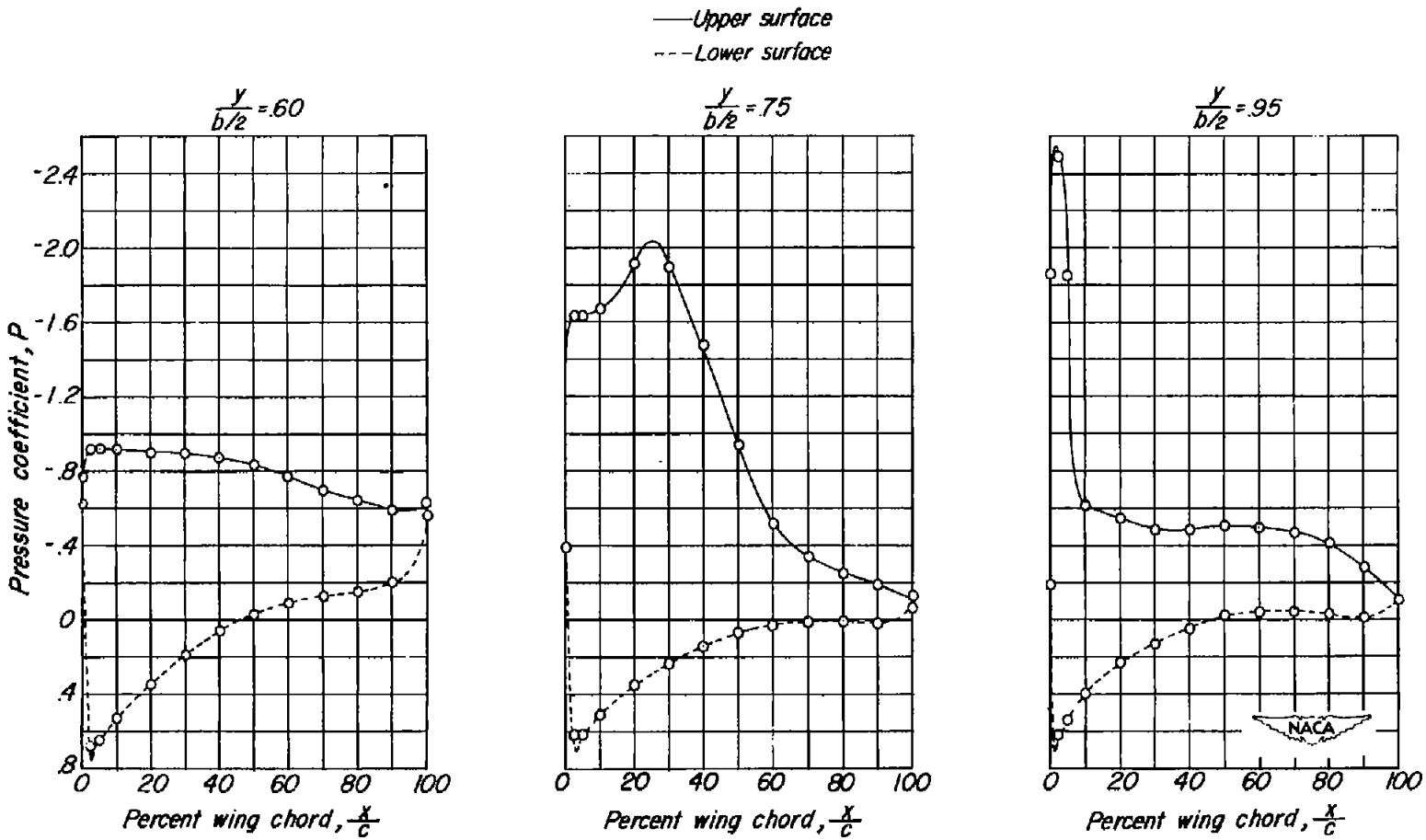

Figure 11.- Concluded.

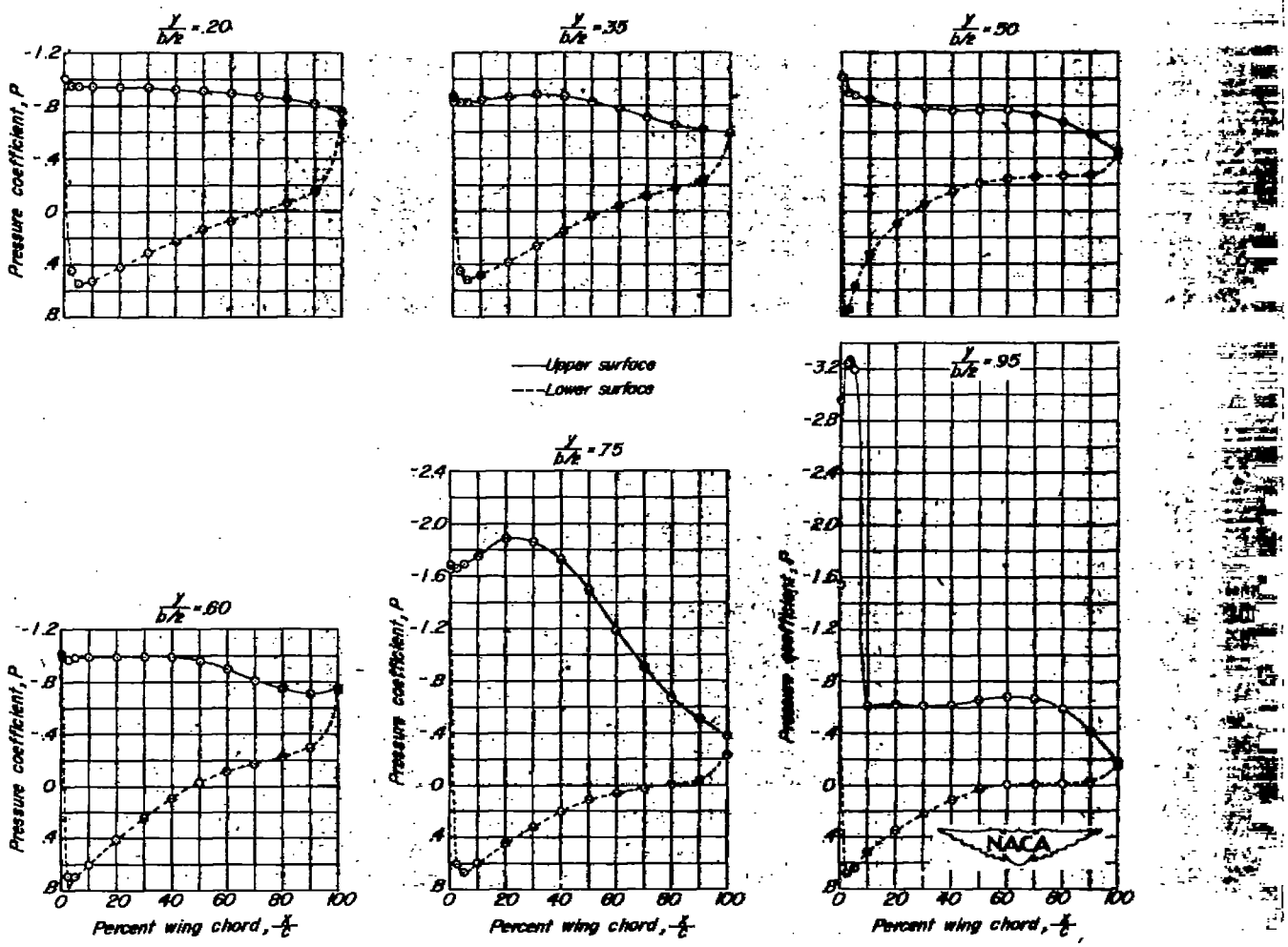

Figure 12.- Pressure distribution on the wing. $\alpha = 20.8^{\circ}$; $\beta = 0^{\circ}$.

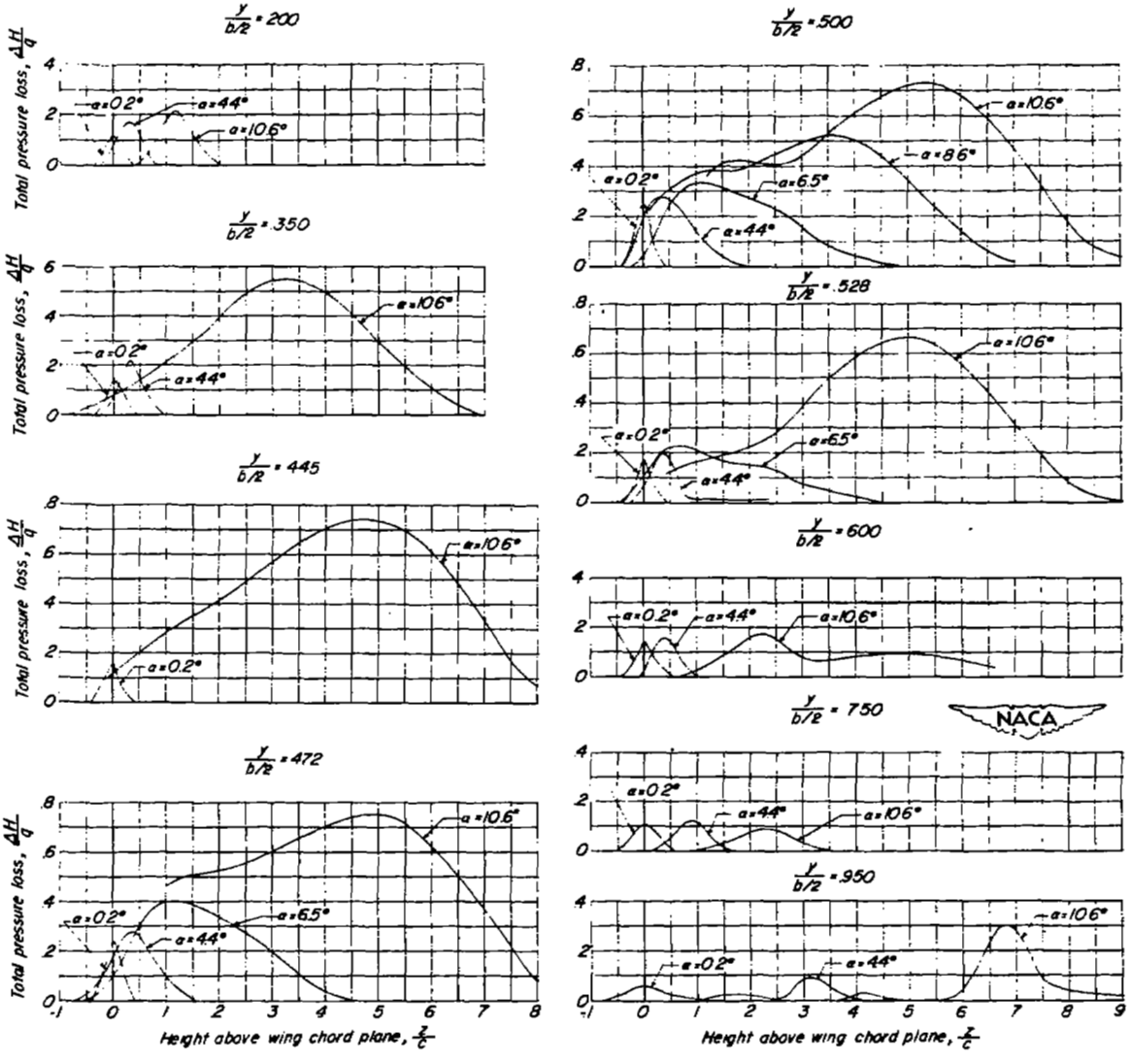

Figure 13.- The effect of angle of attack on the total pressure loss. $\xi = 0^{\circ}$.

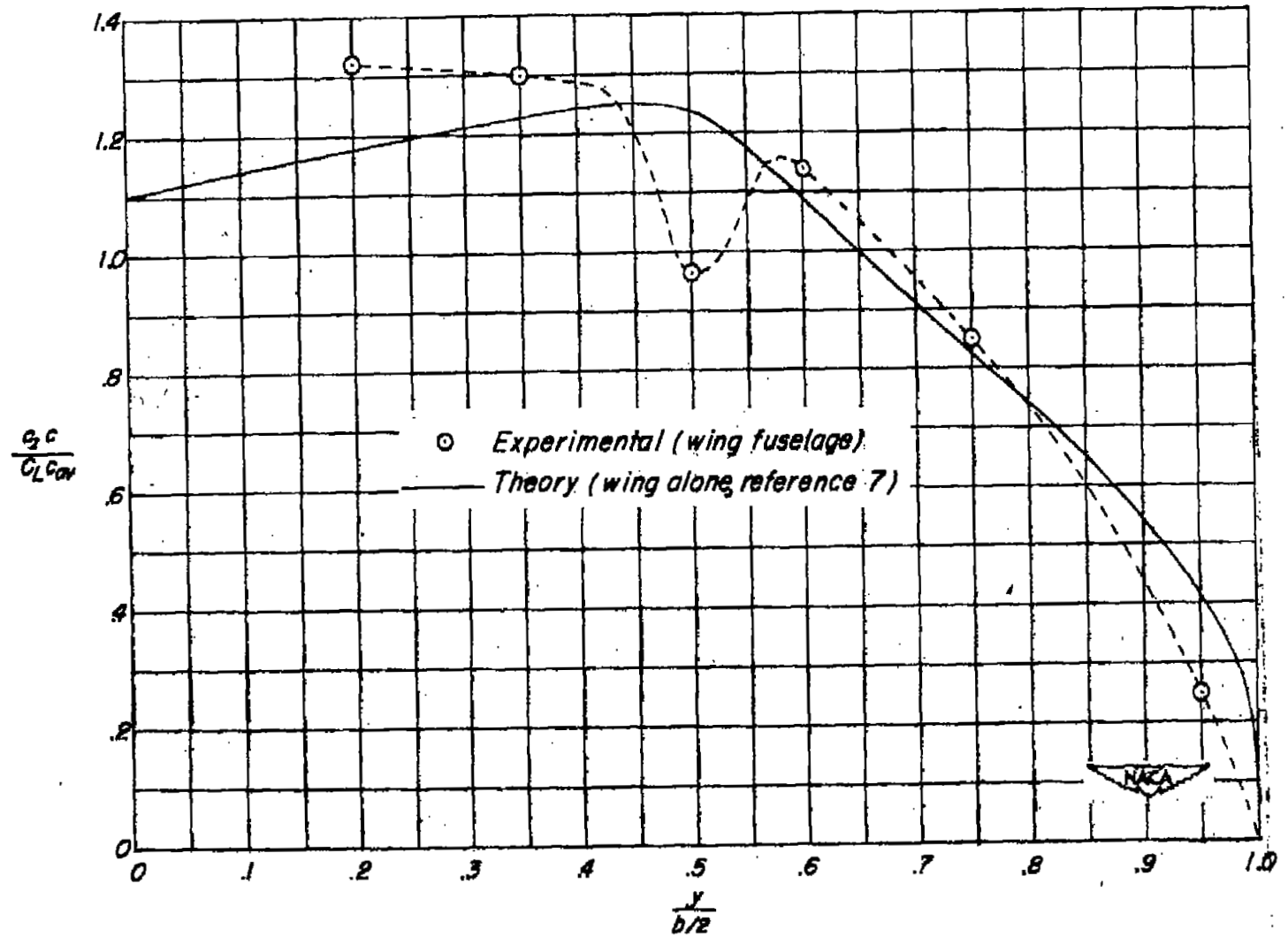

Figure 14.- Experimental and theoretical spanwise load distribution. $\alpha = 2.3^{\circ}$.

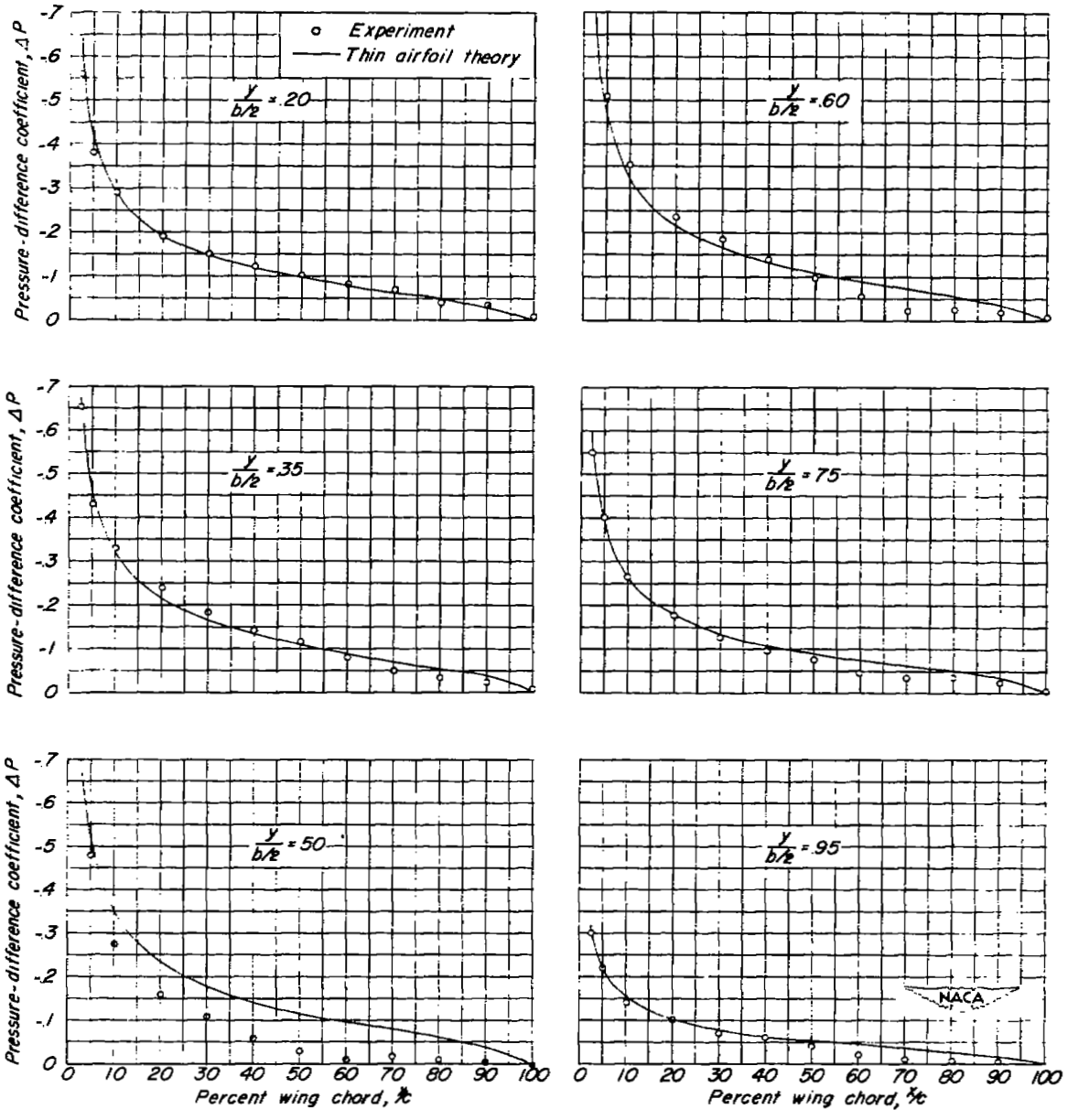

Figure 15.- Experimental and theoretical chordwise loadings. $\alpha = 2.3^{\circ}$.

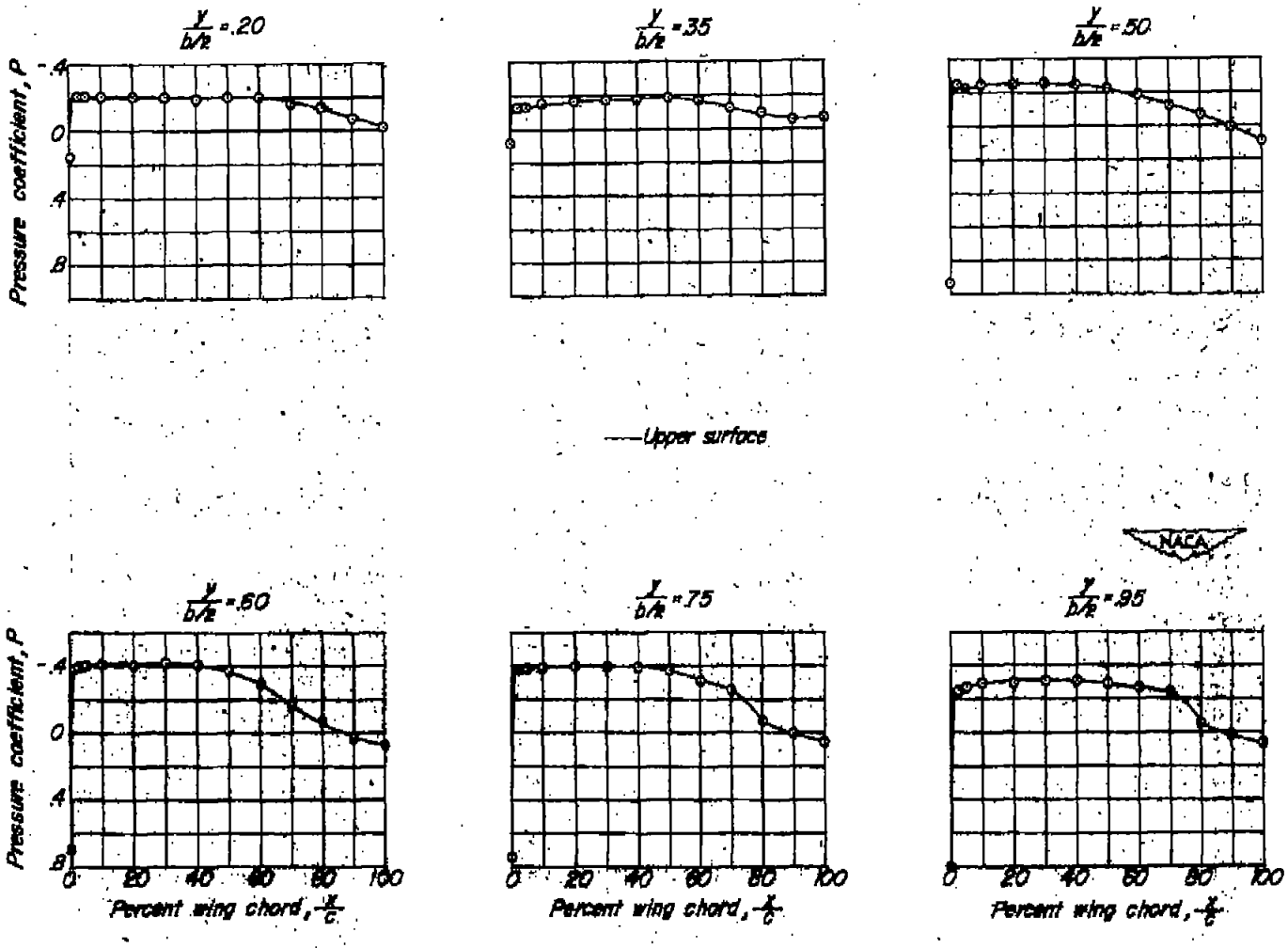

(a) $\beta = -20^{\circ}$.

Figure 16.- Chordwise pressure distribution of various spanwise stations. Data presented with respect to right wing. $\alpha = 0.2^{\circ}$.

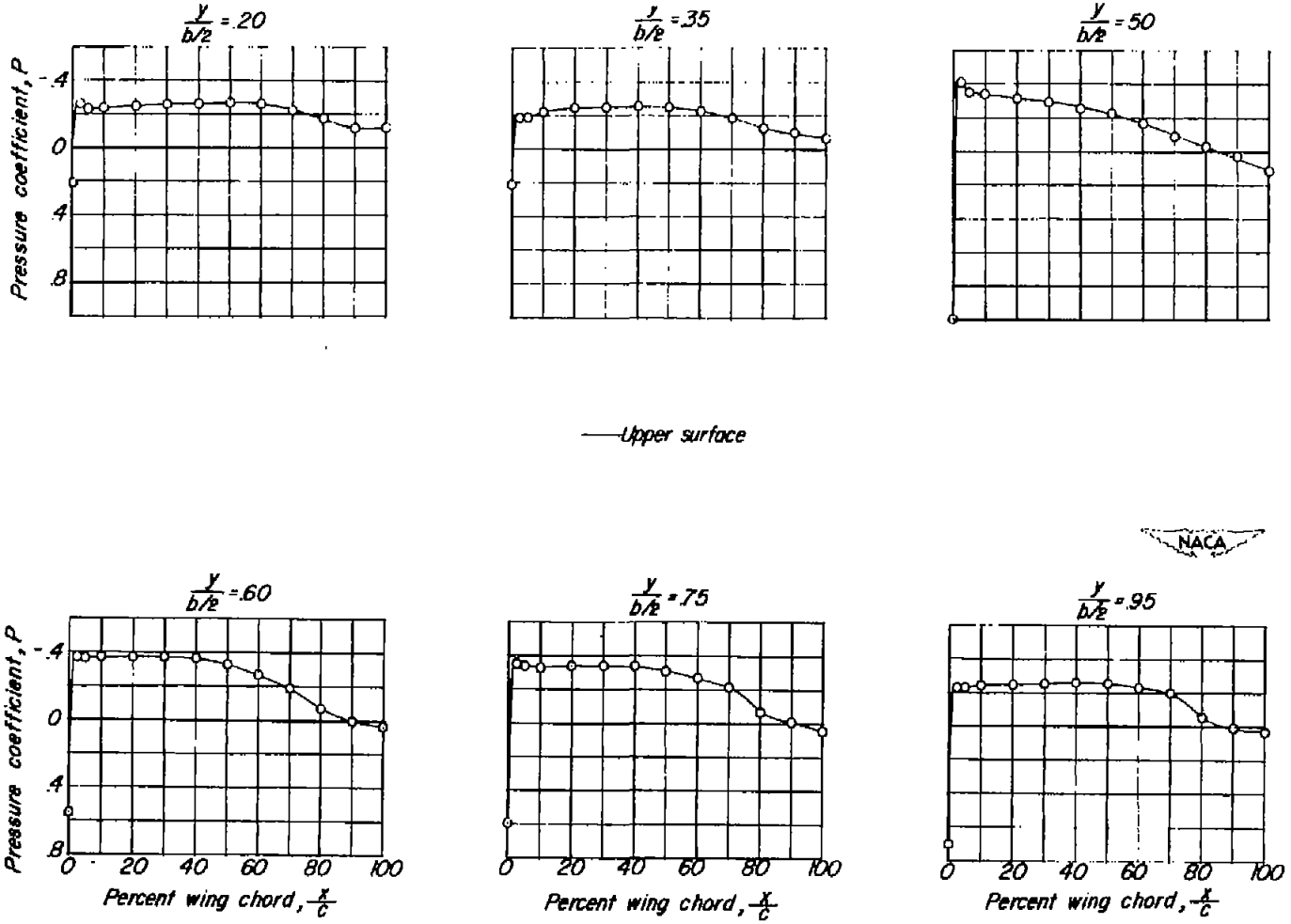

(b) $\beta = -10^{\circ}$.

Figure 16.- Continued.

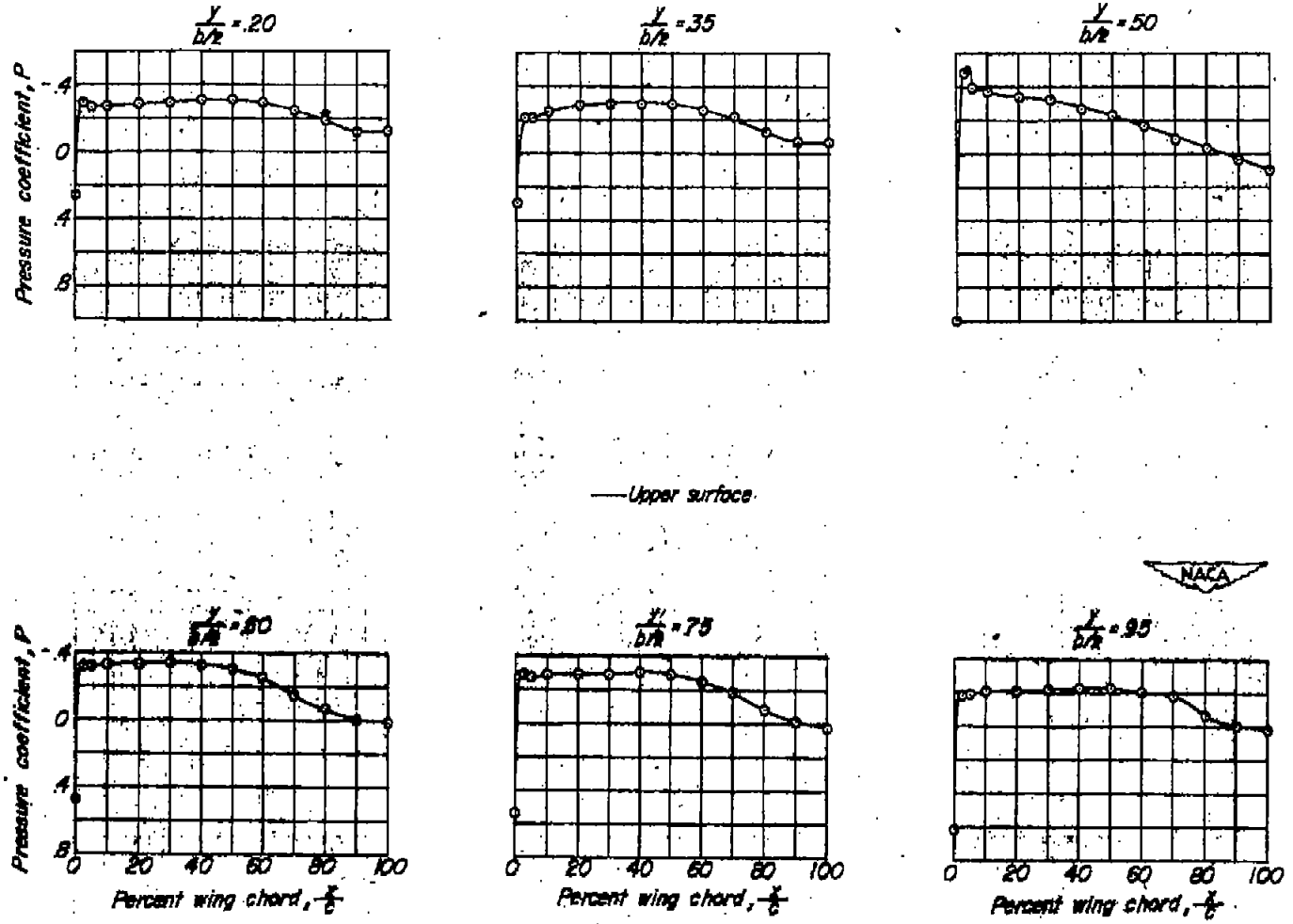

(c) $\beta = -5^{\circ}$.

Figure 16.- Continued.

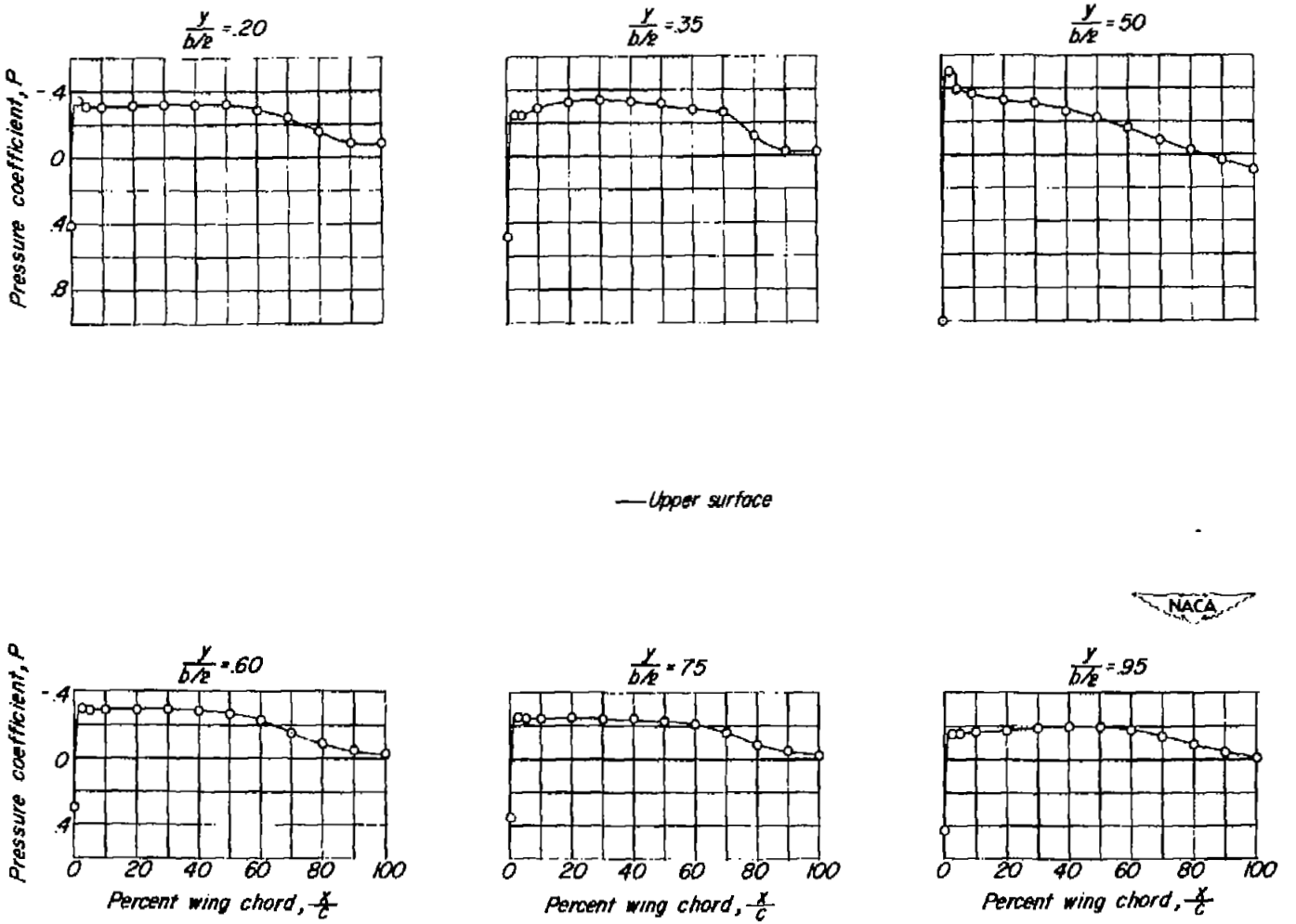

(d) $\beta = 5^{\circ}$.

Figure 16.- Continued.

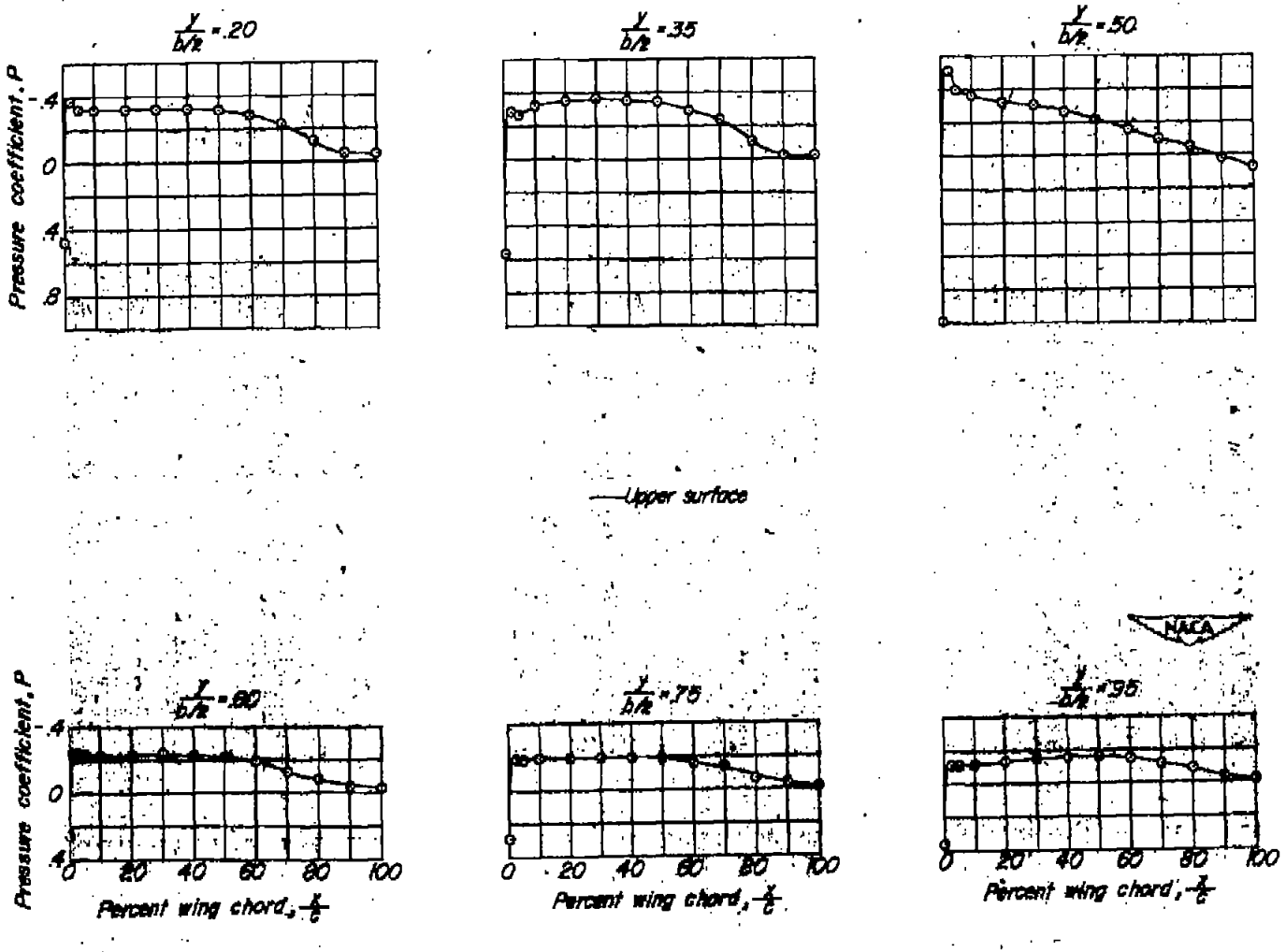

(e) $\beta = 10^{\circ}$.

Figure 16.- Continued.

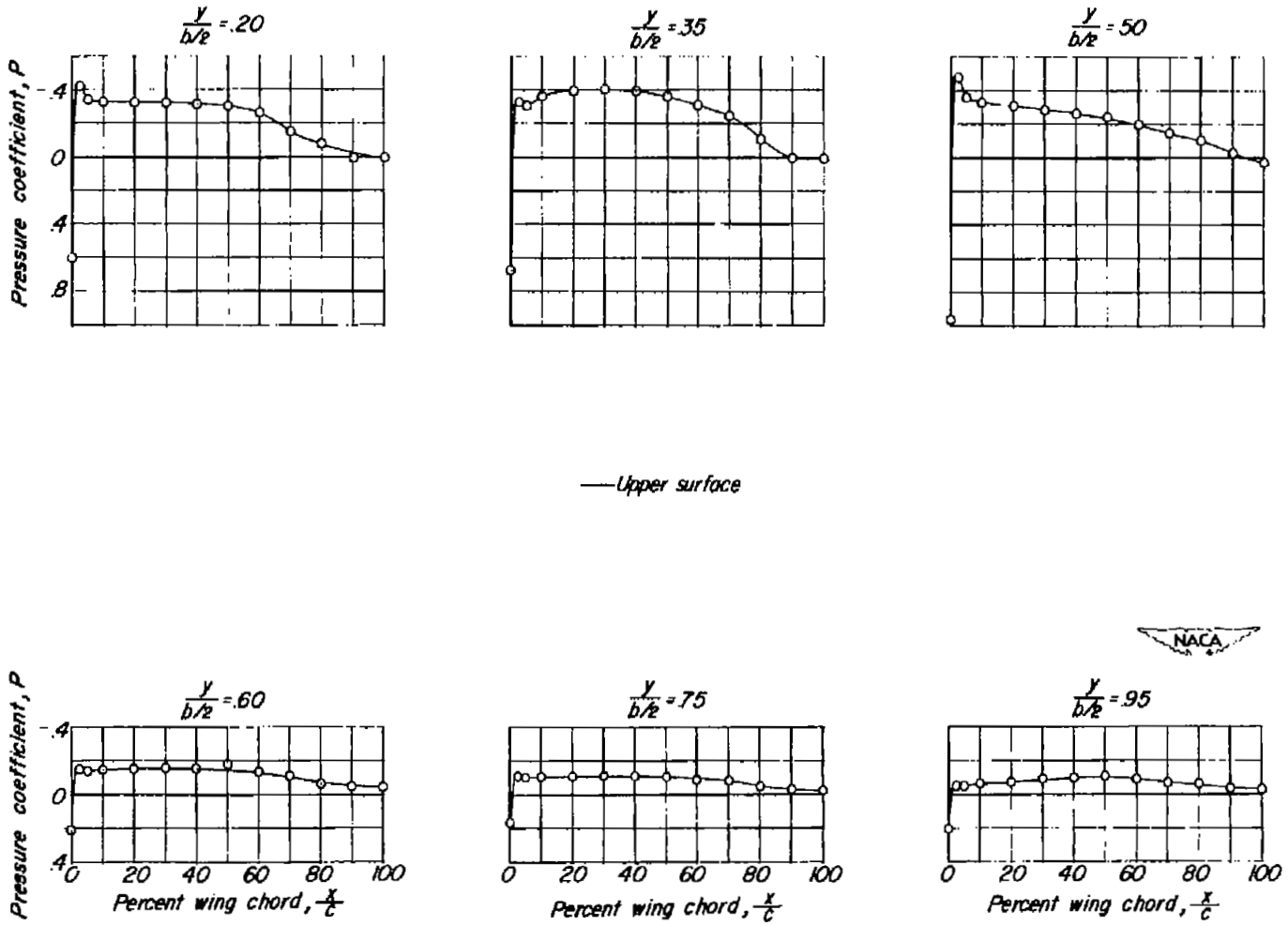

(f) $\beta = 20^{\circ}$.

Figure 16.- Concluded.

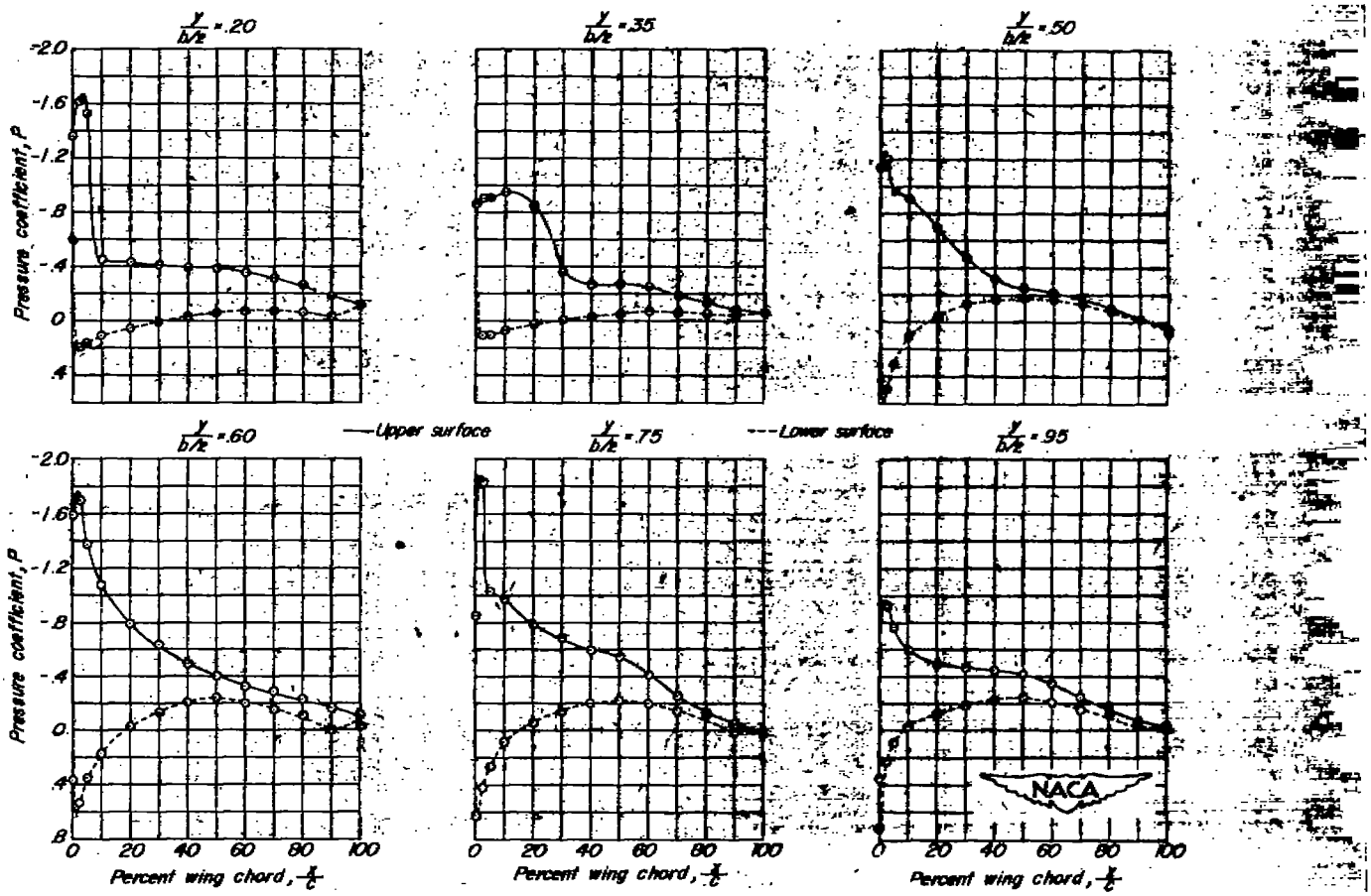

(a) $\beta = -20^{\circ}$.

Figure 17.- Chordwise pressure distribution at various spanwise stations. Data presented with respect to right wing. $\alpha = 6.5^{\circ}$.

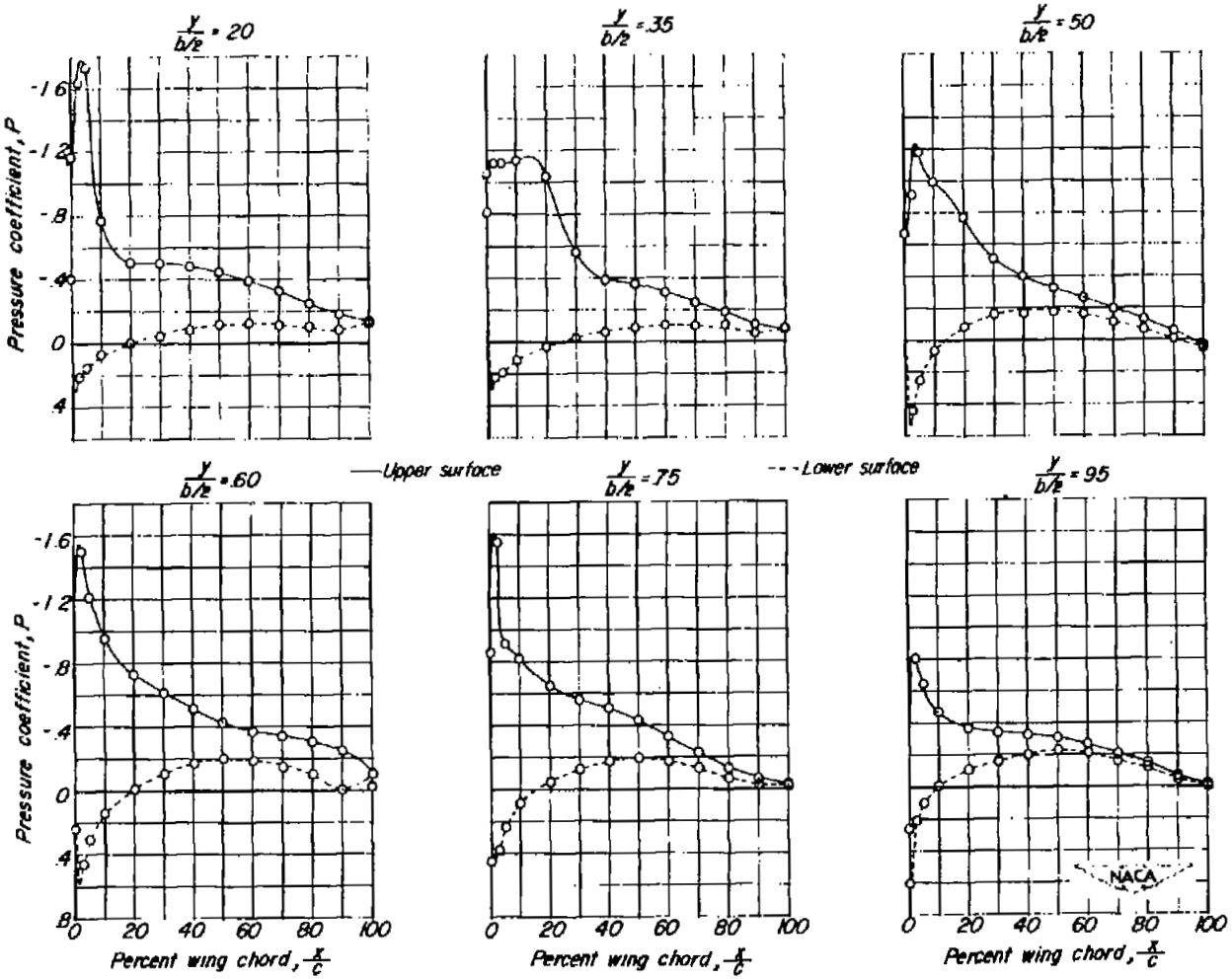

(b) $\beta = -10^{\circ}$.

Figure 17.- Continued.

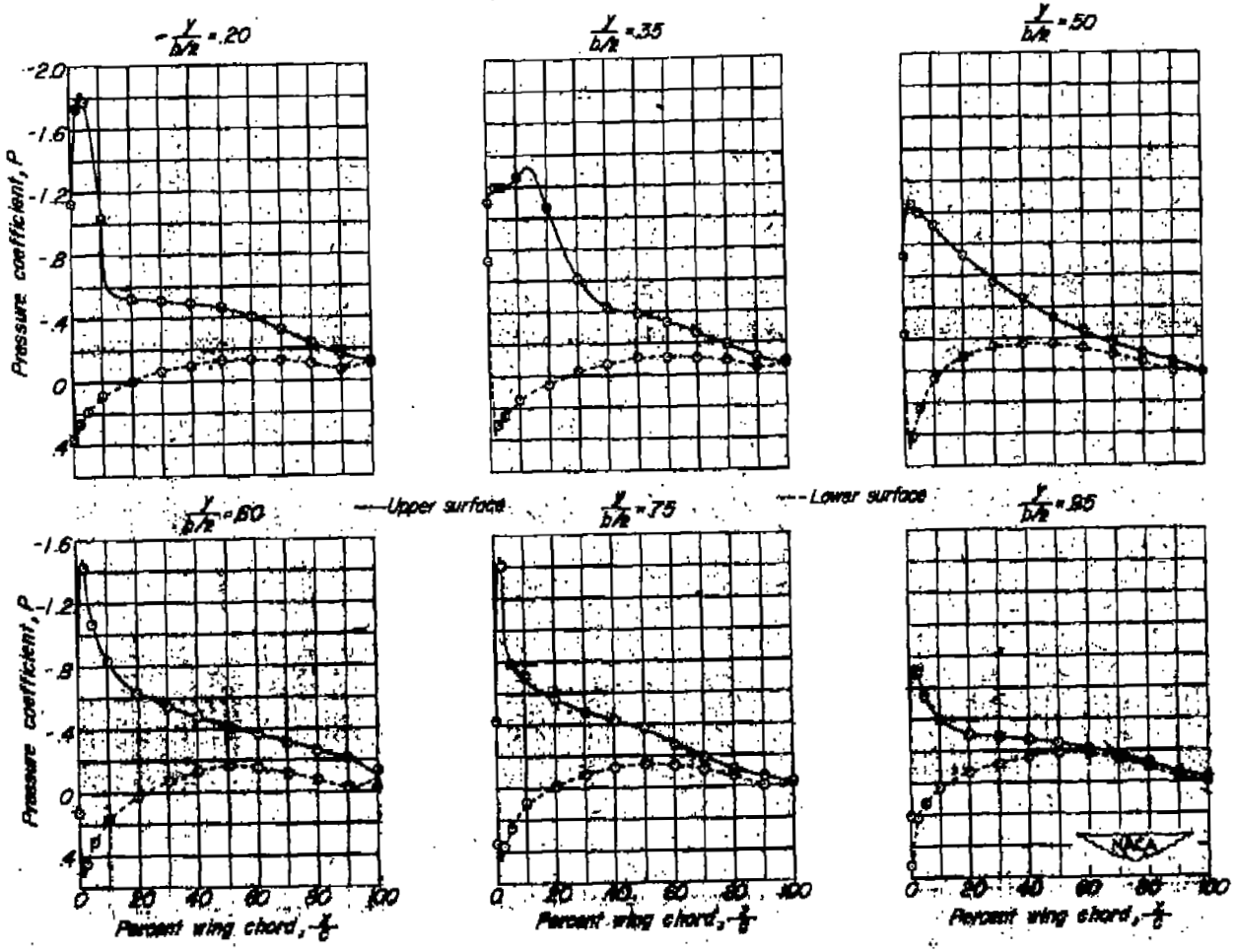

(c) $\beta = -5^{\circ}$.

Figure 17.- Continued.

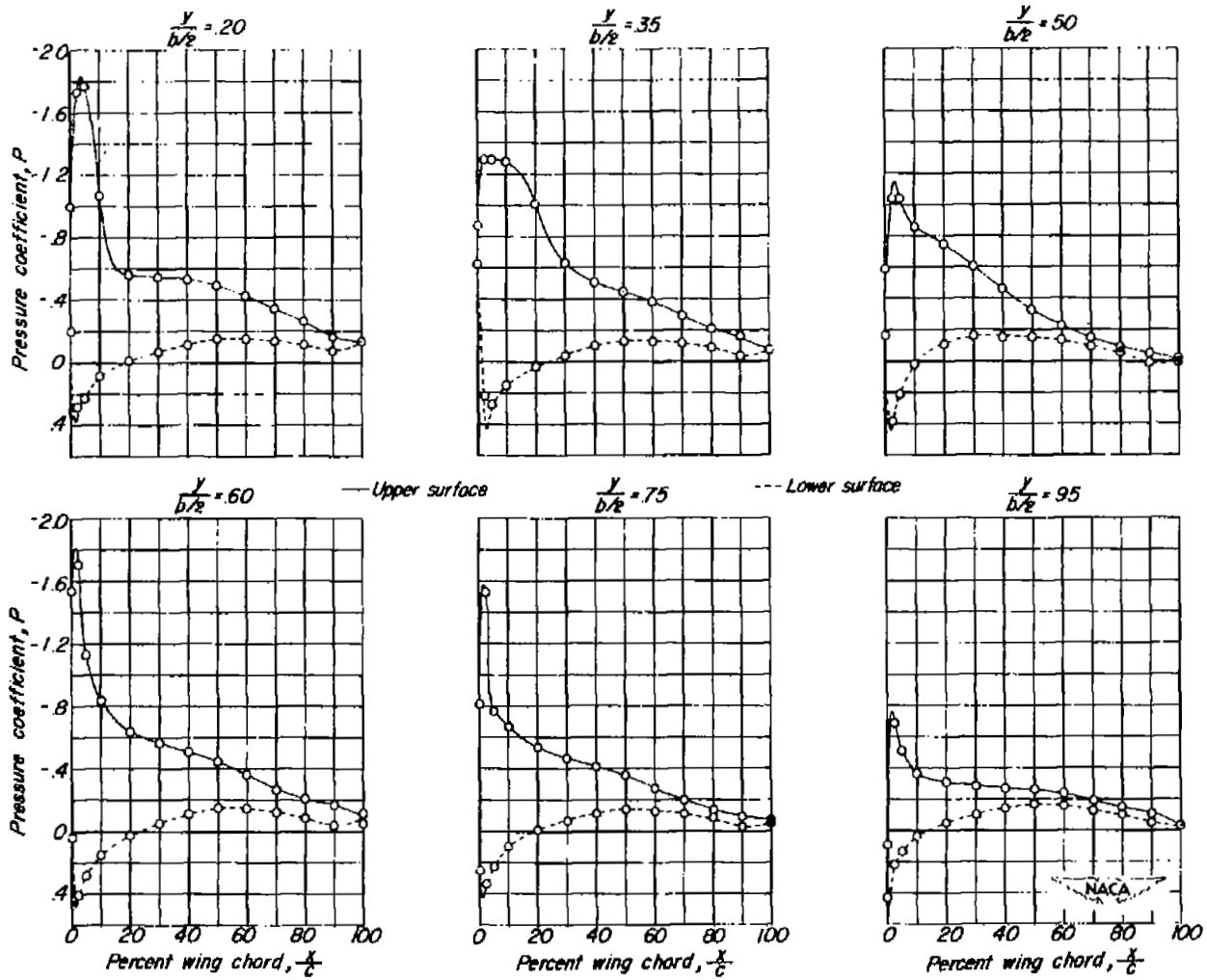

(d) $\beta = 0^{\circ}$.

Figure 17.- Continued.

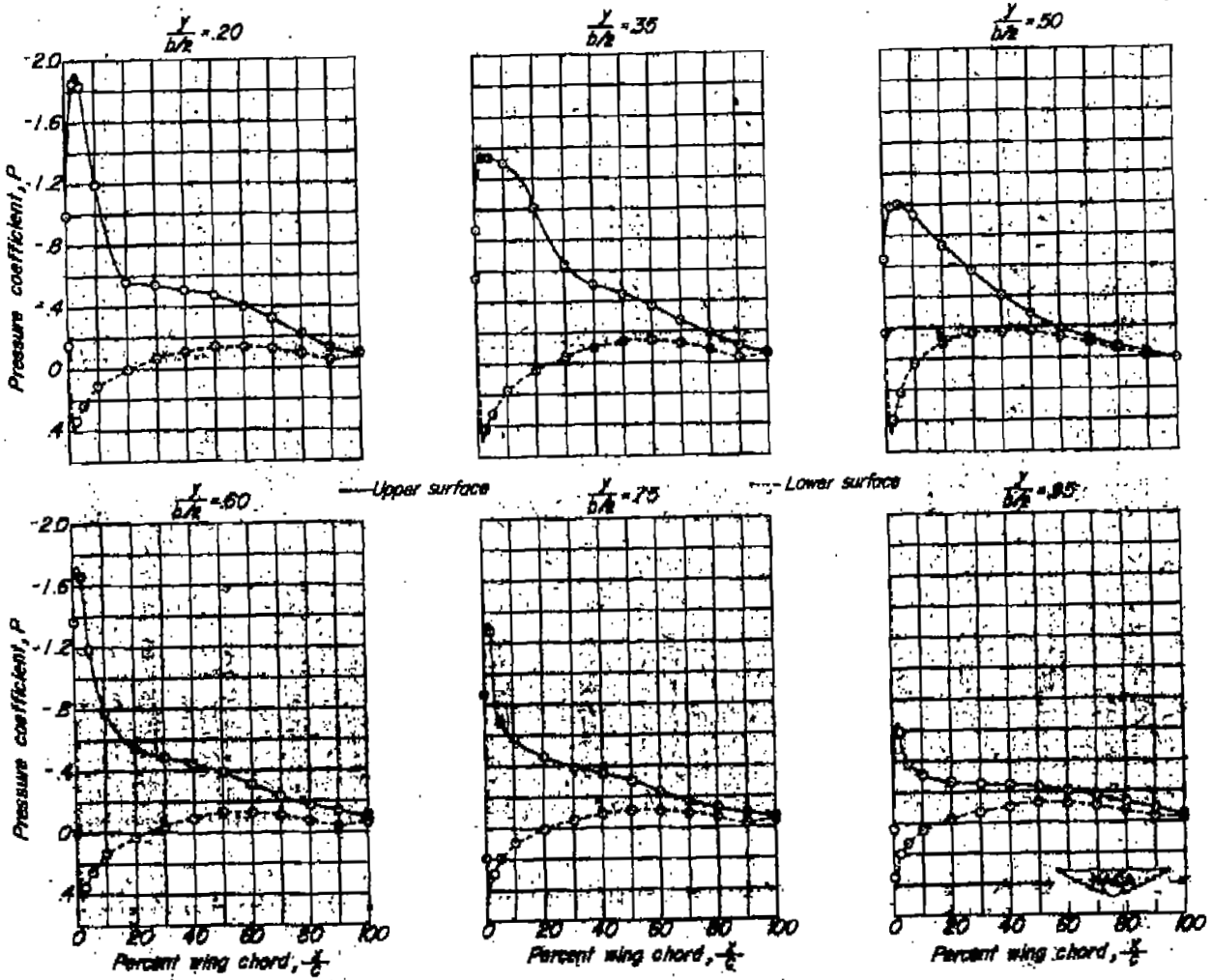

(e) $\beta = 5°$.

Figure 17.- Continued.

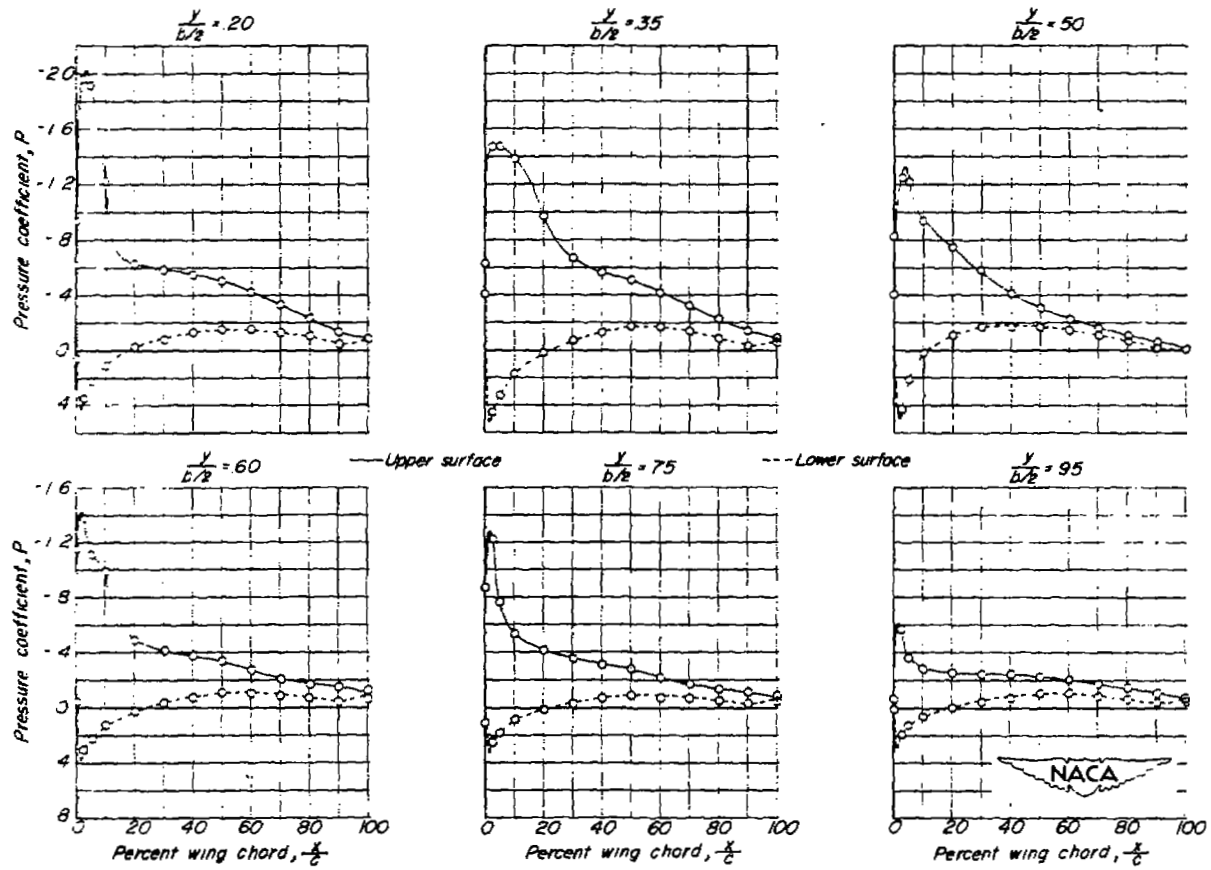

(f) $\beta = 10^{\circ}$.

Figure 17.- Continued.

[redacted]

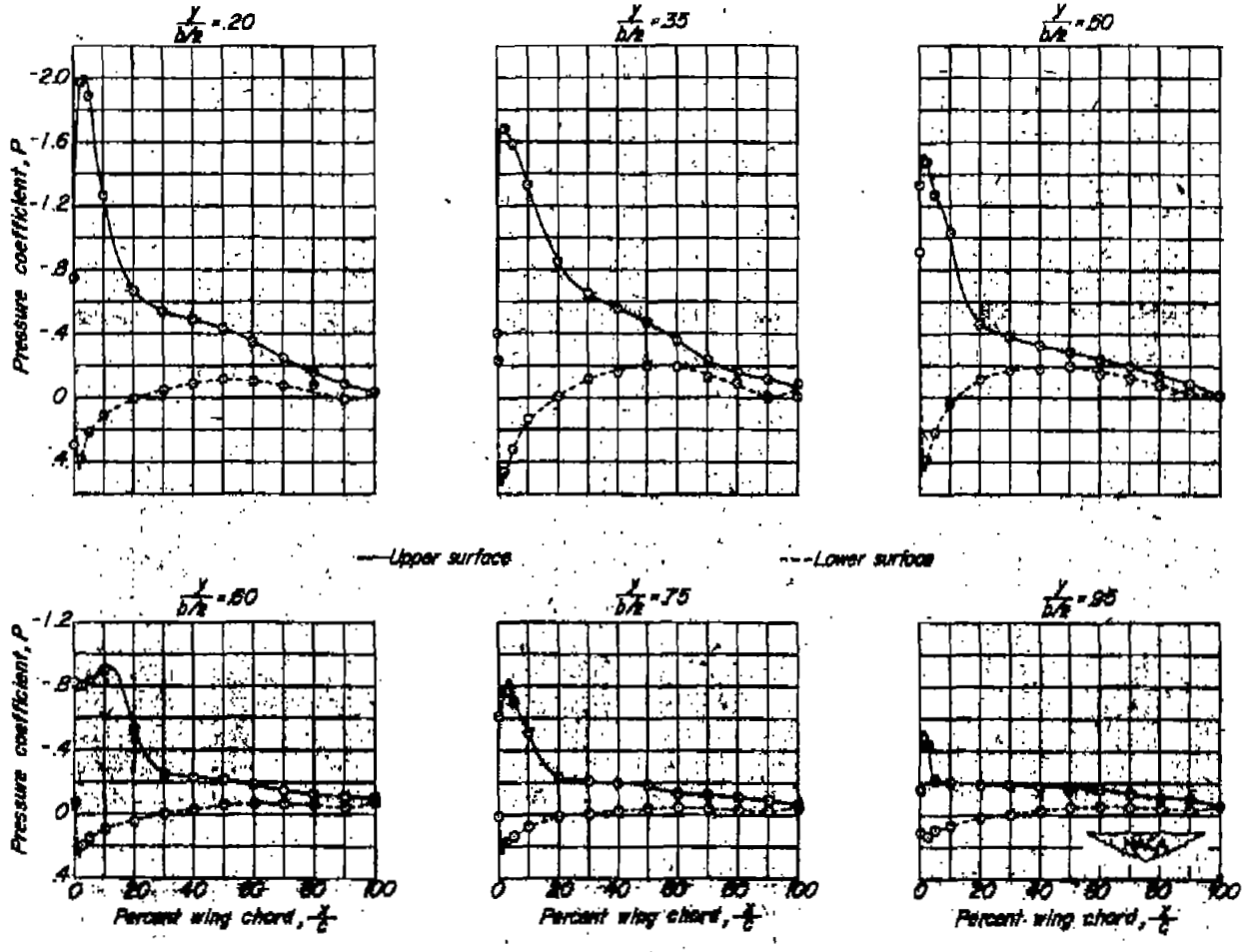

(g) $\beta = 20°$.

Figure 17.- Concluded.

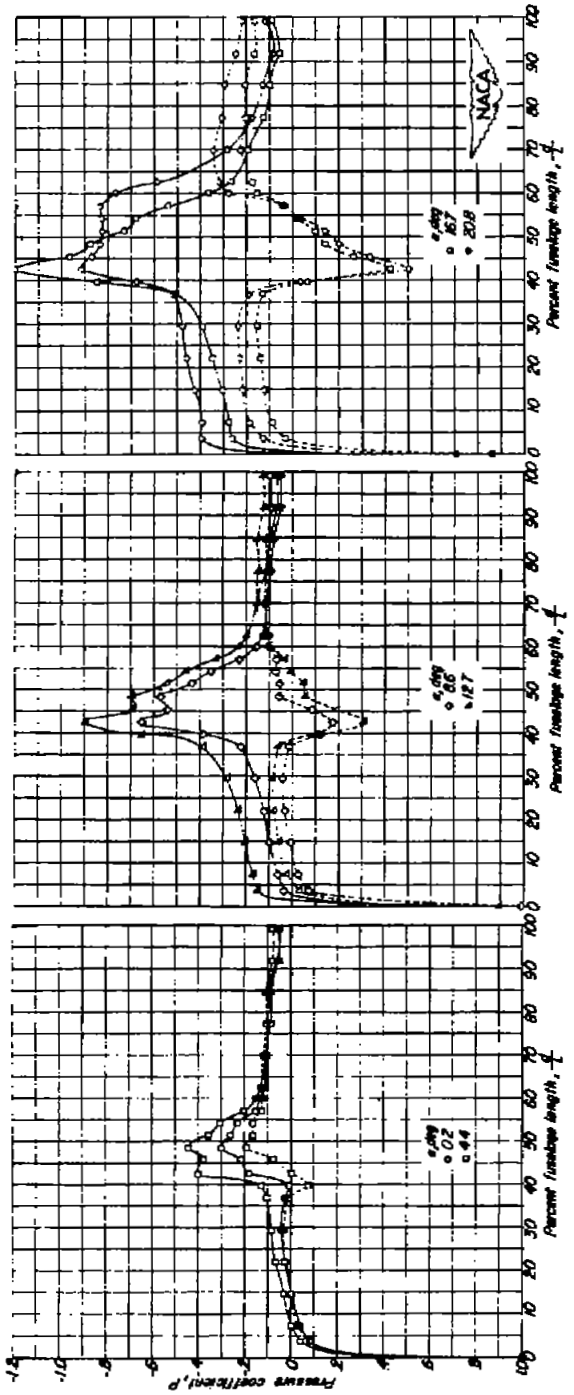

Figure 18.- Pressure distribution on the fuselage in presence of the wing. $\beta = 0^{\circ}$.

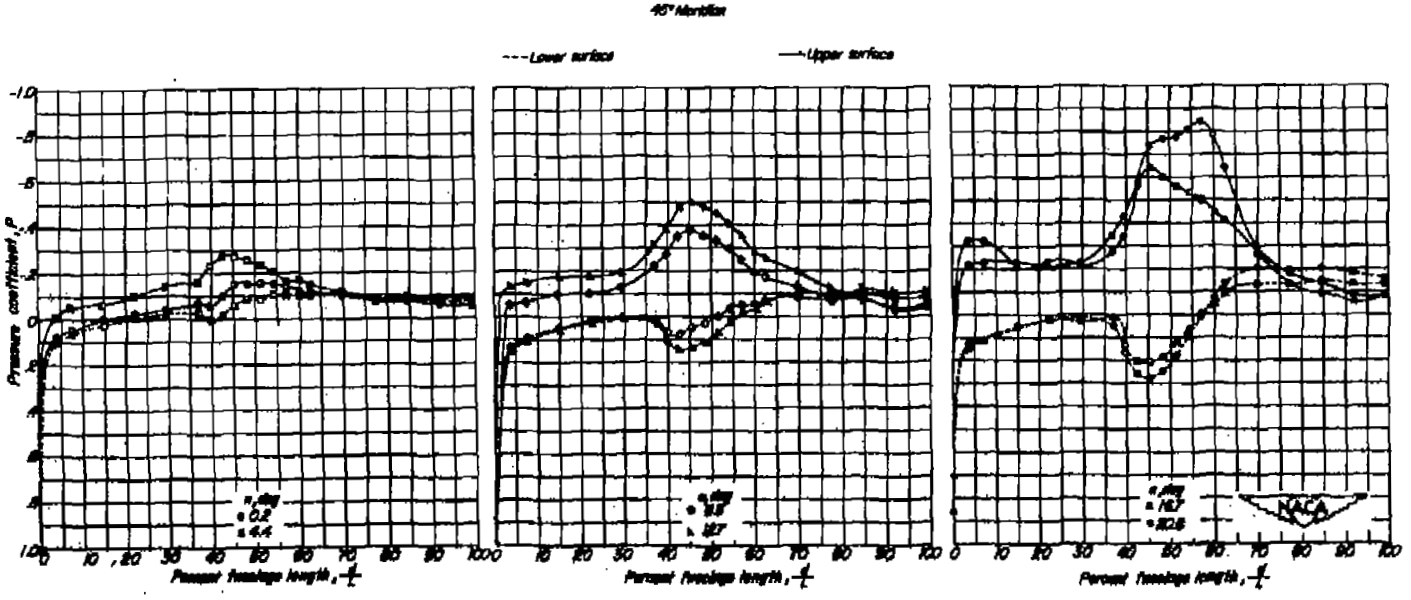

Figure 18.- Continued.

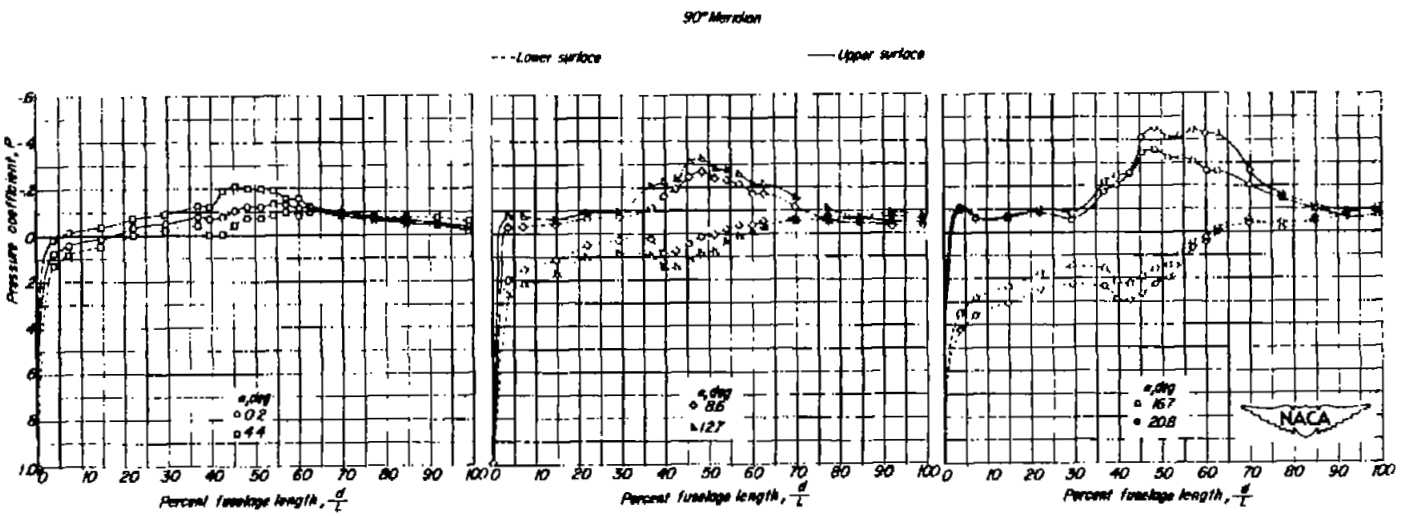

Figure 18.- Concluded.

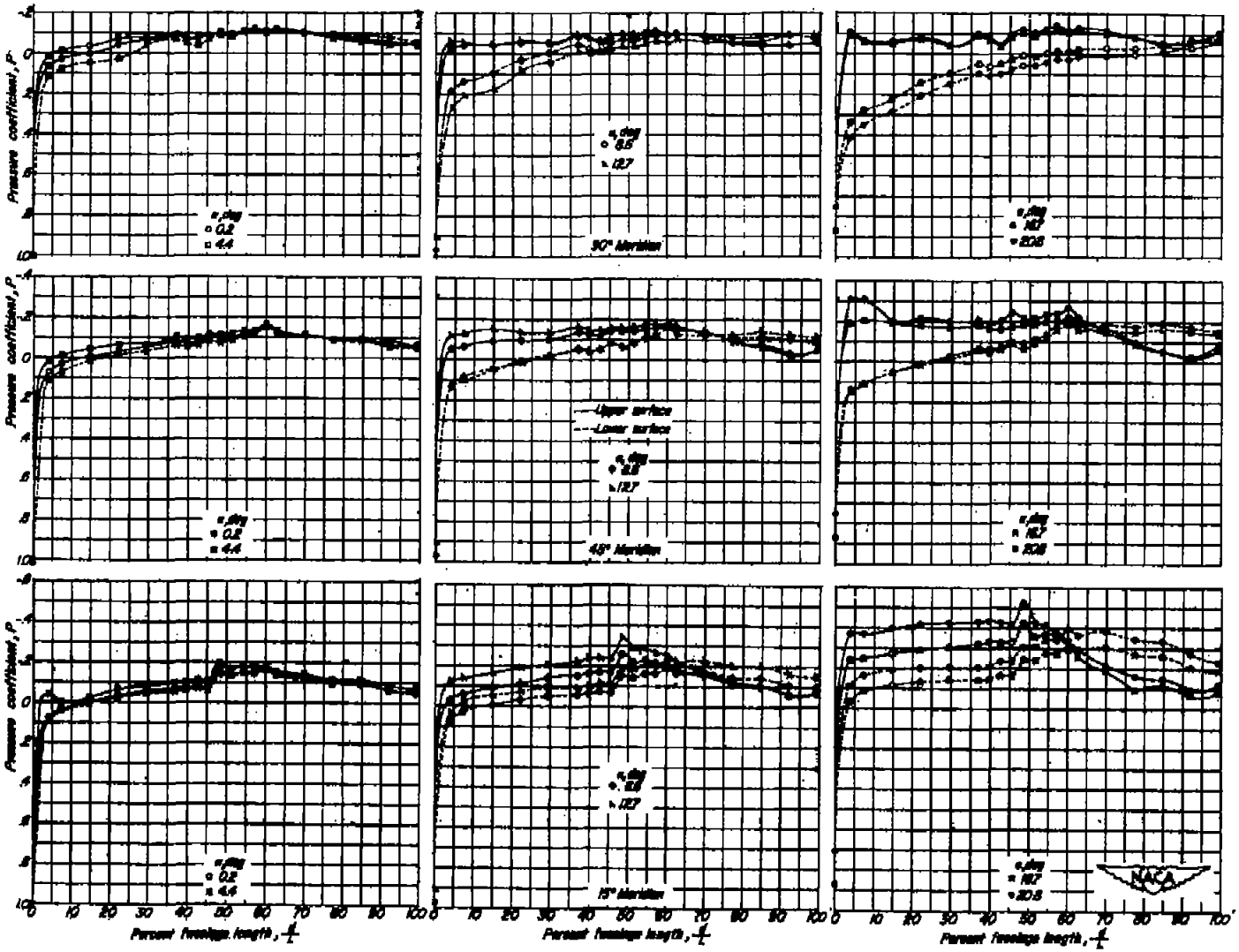

Figure 19.- Pressure distribution on the fuselage alone. $\beta = 0°$.

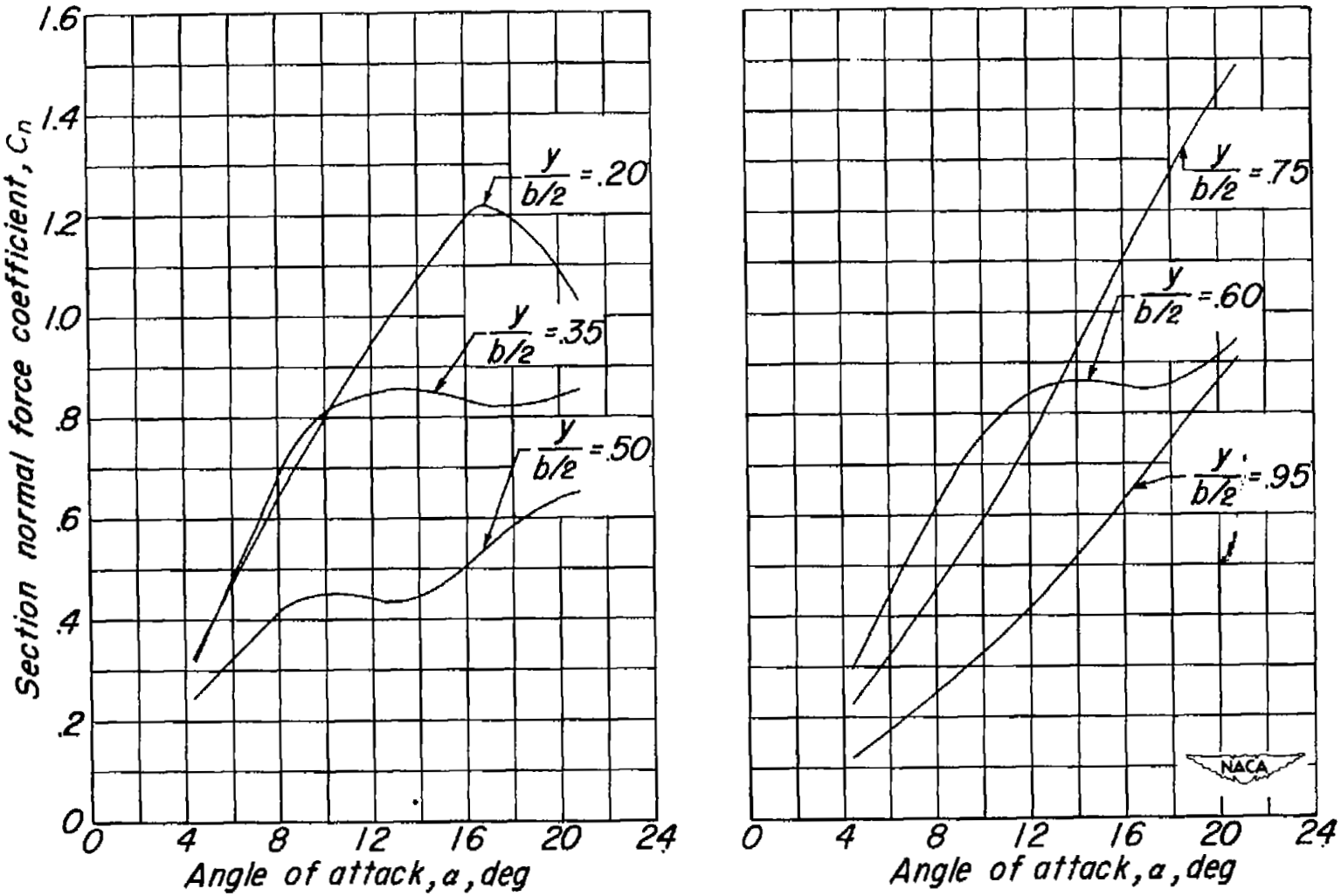

Figure 20.- Wing section characteristics. $\beta = 0^{\circ}$.

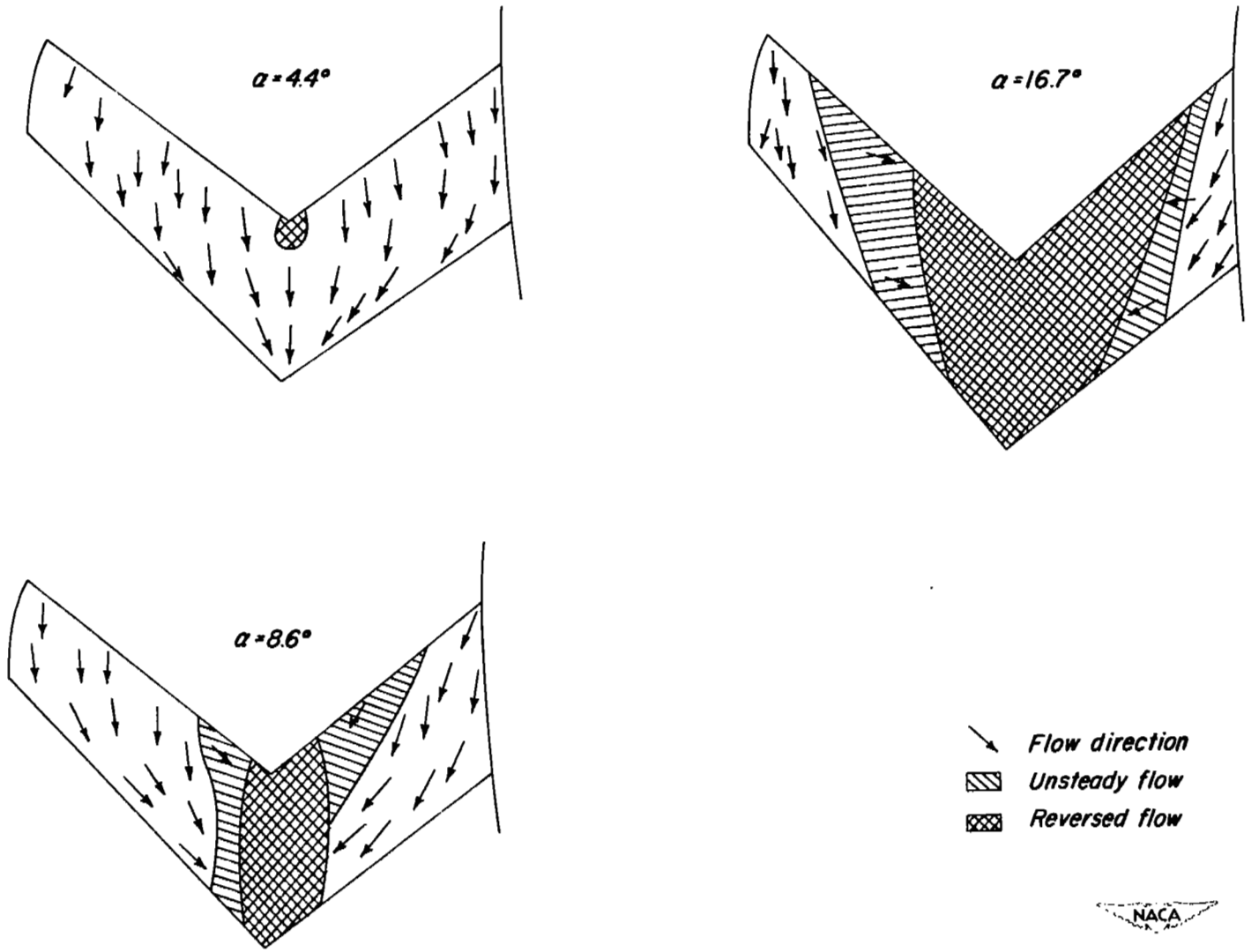

Figure 21.- The effect of angle of attack on the flow characteristics of the wing. $\beta = 0^{\circ}$.

NACA-Langley - 8-7-52 - 300